Journal of Materials Chemistry C

Accepted Manuscript

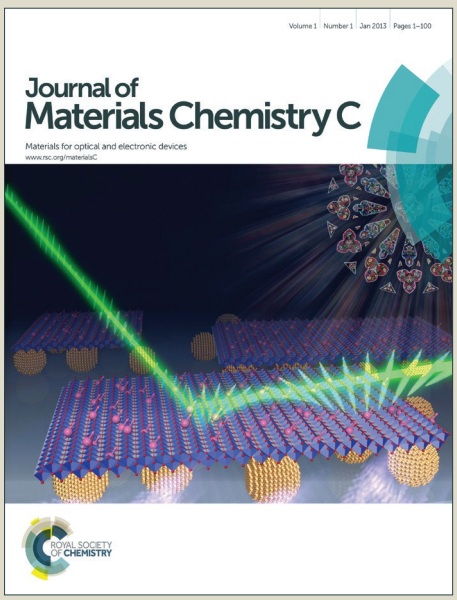

ROYAL SOCIETY OF CHEMISTRY

www.rsc.org/materialsC

Journal Name

ARTICLE

Mastering Heterostructured Colloidal Nanocrystal Properties for Light Emitting Diodes and Solar Cells

Y Received 00th January 20xx,
Accepted 00th January 20xx

DOI: 10.1039/x0xx00000x

www.rsc.org/

R. Mastria [a] and A. Rizzo*[b]

Solution-grown colloidal nanocrystal (NC) materials represent ideal candidate for optoelectronic devices, due to the flexibility with which they can be synthesized, the ease with which they can be processed for device-fabrication purposes and, foremost, for their excellent and size-dependent tunable optical properties, such as high photoluminescence (PL) quantum yield, color purity, and broad absorption spectra up to the near infrared. The advent of surfactant-assisted synthesis of thermodynamically stable colloidal solutions of NCs has led to peerless results in terms of uniform size distribution, composition, rational shape-design and possibility to build heterostructured NCs (HNCs) comprising two or more different materials joined together. By tailoring the composition, shape and size of each component, HNCs with gradually higher levels of complexity have been conceived and realized endowing them with outstanding characteristic and optoelectronic properties.

In this review, we discuss the recent advances in the design of HNCs for efficient light emitting diodes (LEDs) and photovoltaic (PV) solar cell devices. In particular, we will focus on material requirement to obtain superior optoelectronic quality and efficient devices as well as their preparation and processing potential and limitations.

1. Introduction

Surfactant assisted techniques allows the growth of semiconductors, metal, metal oxide and alkaline rare-earth NCs with high crystalline quality, almost free from defects and narrow size distribution.[1–3] By a facile modification of the synthetic protocols, NCs with desired properties could be obtained on purposely designed for disparate applications: fast optical switches,[4] spintronic,[5] transistors,[6] magnetic field driven,[7] and optoelectronic devices,[8,9] low-threshold lasers,[10] and biological labelling.[11,12]

In this frame, electrically driven LEDs and solar cells based on colloidally synthesized inorganic semiconductor NCs represent a completely new technology platform for the realization of flat-panel displays/lighting systems and flexible photovoltaic devices at a low cost.[13,14] The successful application of NCs in LED and solar cell technology relies on the versatility of the colloidal synthesis technique and the excellent optical properties of NC, including tuneable saturated color emission across the UV-visible-near IR range, high PL quantum yield and long term chemical/optical stability.[15] These characteristics have paved the way to the implementation of hybrid devices in which the low-cost, flexible technology of organic materials is combined with the long operating lifetime of inorganic semiconductor devices.

In order to improve the optoelectronic quality, NC surface is ameliorated by epitaxially growing a wider band-gap semiconductor shell, forming a core/shell HNCs. Such an approach offers the unique opportunity to create novel optoelectronic properties by using semiconductor HNCs, instead of single composition material.[16,17] Depending on the energy level alignment of the two adjoined materials, different carrier-localization regimes can be obtained. Since in the strong confinement regime the size and dimensionality dictate the position and the density of energy, a careful design of the composition, size and shape of each component can modify the energy offsets in semiconductor HNCs.

Concerning LEDs, the first demonstration of electroluminescence (EL) using quantum dot (QD) NCs dates back to 1994,[18] and the highest reported external quantum efficiency (EQE) of 20.5%[19] for red emitting QD NC based LEDs is very recent. Non-radiative trap-assisted recombination, Auger annihilation with free carries and electric field induced PL quenching needs to be contained.[20] The challenge is to develop stable NC emitters with high PL quantum yield in the combined presence of charge carriers and electric field. In order to the reach this target, several progress in engineering HNCs for LED application have been made, allowing passivation of defect, suppression of the Auger losses and obtaining unprecedented color purity.

[a] Dipartimento di Matematica e Fisica "E. De Giorgi", Università del Salento, Via per Arnesano, 73100 Lecce, Italy
[b] CNR-Nanotec - Istituto di Nanotecnologia, Polo di Nanotecnologia c/o Campus Ecotekne, via Monteroni, 73100 Lecce, Italy.

† Footnotes relating to the title and/or authors should appear here.

Electronic Supplementary Information (ESI) available: [details of any supplementary information available should be included here]. See DOI: 10.1039/x0xx00000x

Notwithstanding the several progress of HNCs for LED applications, few reports are focused on solution phase syntheses of HNCs of high optoelectronic quality for photovoltaic devices.[9,21] Significant efforts have been addressed to the engineering of NC solar cell architectures mainly based on PbS or PbSe single material.[22] Different structures have been proposed including Schottky-like diode junction,[23] depletion heterojunction,[24,25] hybrid bulk heterojunction structures,[26,27] and QD sensitized solar cells.[28] By analogy with LEDs, solar cells can potentially profit from the heterostructuring strategy, since the reduction of surface trap density is essential to improve both Jsc and Voc values by mitigating charge carrier recombination losses.[26,29] In the last part of the review we will show how the design of HNCs can be exploited as an interesting and promising opportunity to improve the performance of NC based solar cells.

2. Carrier Localization Regimes and Optical Properties

The quantum confinement effect governs the optical and electronic properties of NCs resulting in size and shape dependent characteristics.[30,31] As the dimensions of nanostructure decrease, reaching a value below the exciton Bohr radius, characteristic of each bulk material, the spatial confinement effect induces the quantization of the electronic states and energy band-gap (Figure 1). Therefore, by changing size, composition and shape, it is possible to tune the NC optical properties over a wide spectral range; colloidal chemistry methods allows obtaining this in a cheap, scalable and highly efficient way. Figure 1b-c shows and example of size dependent PL emission of CdSe/ZnS based spherical NCs across the visible spectrum.

Colloidal NCs are usually synthetized by the thermal decomposition of precursors materials in a hot reaction media containing surfactant molecules (i.e. fatty acids, fatty amines, alkylphosphonic acid, or trialkylphosphine),[32,33] which dynamically overcoat and guide the growth ensuring their stability and dispersion in the most common solvents. As a result, NCs prepared by means surfactant-assisted colloidal synthesis can be deposited by low-cost solution-based deposition techniques, such as spin-coating, inkjet printing, and roll-to-roll casting, instead of the more expensive and less versatile vacuum- assisted processes.[34–36]

The resulting nanocrystalline material performances and optoelectronic quality is strongly influenced by the presence of both anionic and cationic un-passivated sites on the surface (dangling bonds) originating from the breakdown of the periodic crystal lattice.[37] An inefficient passivation of these sites could lead to material photoxidation and instability at ambient conditions and moisture. Furthermore, because surface sites are energetically localized within the NC band-gap, they usually act as charge trapping-states thus heavily affecting the charge separation and recombination dynamics.[29,38,39] Relaxation into such localized surface states diminishes the overlap between the electron and hole wavefunctions, reducing the probability of radiative recombination events. In addition, surface defects form even deeper energy trap states lead to strong carrier localization and to nonradiative exciton relaxation processes. Therefore, surface chemistry and passivation in these systems assume a preeminent role for their successful application in highly efficient optoelectronic devices.

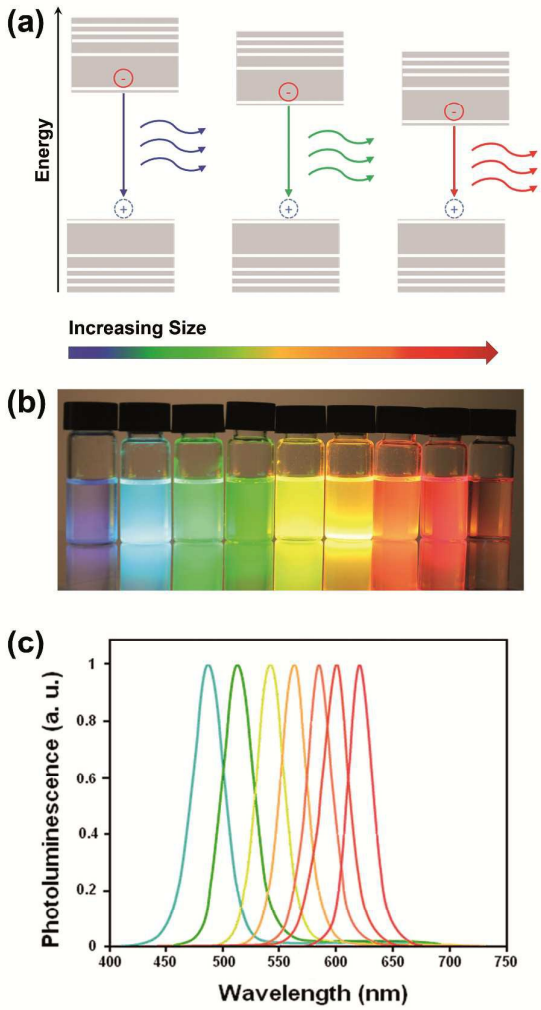

Figure 1. (a) Sketch of the effect of band-gap narrowing by increasing the size of NCs. (b) Suspensions of colloidal CdSe/ZnS core/shell HNCs of different sizes under UV excitation and relative (c) size dependent emission spectra.

In general, organic ligands provide a good degree of surface passivation but their efficacy mainly relies on the stability of the ligand itself and, thus it does not ensure a long-term effect.[40] Organic ligands, indeed, can be distorted during the processing of NCs into films and actual devices, and, in addition, barely passivate at the same time both anionic and cationic surface sites. Moreover, the long and insulating surfactant molecules hinder the efficient charge transport and percolation through NC domains. A powerful way to solve this issue is to overcoat the NC surface with a second inorganic semiconductor material creating the so-called HNCs. In this case, the inorganic coating effectively enables the passivation

of both unsaturated anionic and cationic species. Recent advances in colloidal science have led to the synthesis of HNCs based on several semiconductor materials combined into spherical core/shell quantum dots (QDs), dot-in-rod, rod/rod and branched nanostructures.[32] In addition, compared to single material based NCs, HNCs allow further degree of tuning of their physical properties, such as emission quantum yield and exciton lifetime, which are fundamental parameters for their application in LED and photovoltaic devices. Depending on the energy level alignment of the two materials, different carrier-localization regimes can be obtained. Since in the strong confinement regime the size and dimensionality dictated the position and the density of energy, a careful design of the composition, size and shape of each component can modify the energy offsets in semiconductor HNCs, and in turns the electron-hole wavefunction overlap and material optoelectronic properties.[41] Thus, the thoughtful design of HNCs will lead to obtain the desired photophysic and optoelectronic properties, targeting the different device applications. The relative energy band offset of NHSs can be engineered through the quantum confinement effect also by varying the relative size and shape of each component, as a result, the same core/shell combination of materials can lead to different regimes of charge localization depending on the core size or shell thickness.[42–45]

In general, possible HNCs energy band configurations can be classified as type I, quasi-type II and type II regimes, depending on the relative bulk semiconductor energy levels (Figure 2).[41]

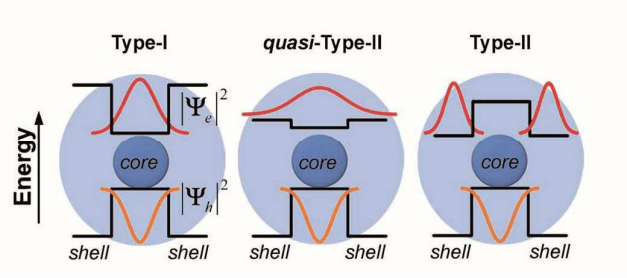

Figure 2. Schematic representation of the energy level alignment and carrier localization in type I, quasi-type II and type II HNCs. The red and orange lines indicate the lowest energy electron and hole wavefunctions, respectively.

This scheme represents three ideal cases of charge carrier distribution, valid only for infinite offsets. Whereas for finite offsets, and especially in HNCs, charge localization regimes are not well defined since the electron and hole wave functions can completely or partially spread throughout the entire NHS. Therefore, the bulk band offset scheme between the two, or more, semiconductors in NHSs should be used merely as a tool to predict in which material the wave function of a given carrier mainly resides.

2.1 HNC Type I-enclosed energy level alignment

The type I is an enclosed alignment in which the band-gap of one component is located entirely within the gap of the other semiconductor. In this configuration, both charge carriers are confined in the narrower band-gap material. Type I HNCs are usually constructed by growing a shell onto preformed NC cores having narrower optical band-gap. Several material combination (CdSe/ZnS,[46,47] CdS/ZnS,[48] CdSe/CdS,[49] InP/ZnS,[50] PbS/CdS[51]) and synthetic protocols have been developed for highly efficient and stable type I HNCs. The growth of a shell having a wider bandgap offers the advantage of protecting the core from the surrounding environment and, thus to preserve its optical properties during oxygen exposure, purification or ligand exchange treatments. As an example, the CdSe NC surface is highly susceptible to photoxidation due to the presence of unpassivated Se sites that can react with oxygen or water molecules. The deleterious effect of surface oxidation causes a broadening and blue shift of the first excitonic peak in the absorption spectrum and, a reduction of the optical density.[47] By overcoating the CdSe core with few monolayer thick ZnS, CdS or ZnSe shells, the density of surface dangling bonds is massively reduced, resulting in enhanced PL quantum yield and in minimized photoxidation.[47] PL studies showed that CdSe core only NCs display a prominent deep-trap emission whose contribution to the whole spectrum is of ~82%, such deep-trap emission is greatly reduced to a contribution of ~4%, ~29% and ~40% for ZnS, CdS and ZnSe shells, respectively.[46] As the deep-trap emission decreases the PL quantum yield increases from ~4% up to ~77% in the case of four monolayer-thick ZnS shell and up to ~82% with a multiple shell made of ZnSe and ZnS, (Figure 3a-d)[46] thus demonstrating that reducing the deep-trap emission is of utmost importance to achieve high PL intensity and saturated color emission.

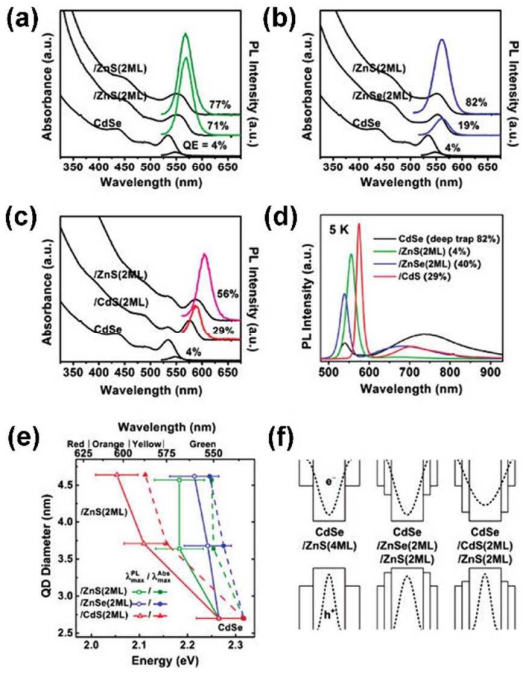

Figure 3. Absorption and emission spectra of CdSe-Based Core/Shell NCs: (a) CdSe/ZnS, (b) CdSe/ZnSe/ZnS, and (c) CdSe/CdS/ZnS nanocrystals and related QE measured relatively to Rhodamine B in methanol (85% QE). (d) PL spectra of core/shell HNCs at 5 K. In parentheses, the percentage of deep trap emission. (e) Variation of the first exciton absorption peak (solid symbols), the emission maximum (open symbols), and the size of nanocrystals. Error bars

represent emission bandwidths (full width at half-maximum). (f) Proposed band-offset for the core/shell structure. Dotted lines illustrate electron and hole wavefunctions. Adapted with permission from ref. [46]. Copyright 2008 American Chemical Society.

Thanks to these properties type I HNCs are among the most investigated as efficient emitters for LED devices.[52,53]

Besides the outstanding emission properties, type I heterostructuring can lead to an enhancement of the UV absorption as well. In CdSe/ZnS QD HNCs, the shell growth causes a red shift of CdSe absorption and emission peaks, resulting from a partial extension of charge carriers into ZnS shell.[47] In CdSe/ZnS HNCs, indeed, while the hole wavefunction remain localized into CdSe core, the electron wavefunction slightly spreads into the ZnS shell (figure 4b),[54] reducing the confinement energy and leading to red-shifted absorption. However, beyond a limit value of the shell thickness, the confinement energies remain constant because the electron and hole wave functions cannot spread out any further. In this regime, although the emission properties are unaffected, the shell thickness variation becomes relevant in charge separation/recombination dynamics and charge transfer mechanisms. Transient absorption spectroscopy measurements on a system consisting of anthroquinone molecules, acting as an electron withdrawing material, adsorbed onto the surface of CdSe/ZnS HNCs reveal that both charge separation and recombination rate decay exponentially by increasing the shell width (Figure 4).[54]

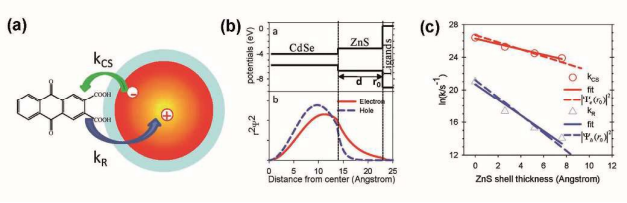

Figure 4 (a) Sketch illustrating the Photoinduced Charge Separation (k_{CS}) and Recombination (k_R) Processes in CdSe/ZnS Core/Shell QD-Anthraquinone Complexes. (b) Band alignments and radial distribution functions for 1S electron and hole levels of CdSe/ZnS core/shell QD with a 13.7 Å CdSe core and 3 monolayers of ZnS shell. Vertical dashed lines indicate CdSe/ZnS and ZnS/organic ligand interfaces. Potentials are relative to the vacuum energy level. (c) Plot of charge separation (open circles) and recombination (open triangles) rates as a function of ZnS shell thickness. Figure also shows the calculated electron (red dashed line) and hole (blue dashed line) densities at the shell surface as a function of shell thickness. Adapted with permission from ref. [54]. Copyright 2010 American Chemical Society.

Charge recombination rate decay faster than separation due to the different hole and electron distribution between the core and the shell (Figure 4). These findings suggest that, in principle, type I HNCs could be exploited to improve charge separation efficiency of a donor/acceptor PV system by simply varying the shell thickness.

2.2 HNC Type II- staggered energy level alignment

The type II arrangement consists in staggered energy level positioning in which both the low energy electrons and holes states are in different semiconductors, thus negative and positive carries are spatially separated and localized in each component material.

Type II band alignment can be achieved with several combination of materials such as CdTe/CdSe,[55] CdSe/ZnTe,[55] CdTe/CdS,[56] ZnTe/CdS,[57] ZnTe/CdTe[57] and CdS/ZnSe.[42] The spatial separation of charge carriers has several implication on the absorption and emission properties, as well as on charge separation and recombination dynamics of HNCs. Typically, the absorption spectra show new optical bands that appear at lower energies, adding up to the contribution of each single component.[58,59] Such bands are related to weak spatially indirect transitions, i. e. charge transfer states, existing at the interface between the two semiconductors, which extend the absorption of the type II HNCs to longer wavelength. Additionally, the PL and absorption of type II HNCs shifts towards lower energies because the effective energy-gap is given by the band offset between the two components and it is independent from the band-gap of the single core and shell material. Thanks to this property, Type II HNCs can be exploited as promising tunable near infrared emitters.[60] As an example, CdTe/CdSe HNCs emission spectrum is peaked at lower energy if compared to the corresponding core, which is completely quenched during the HNC formation.[58] Similar behaviour have also been observed in other type II system such as CdS/ZnSe HNCs.[42]

Besides the effect on the absorption and emission properties, type II band alignment also influence the exciton dynamics (Figure 5).

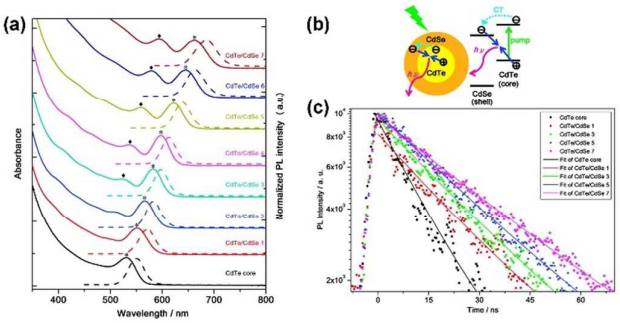

Figure 5. (a) Absorption (solid lines) and PL (dotted lines) spectra of the CdTe cores and CdTe/CdSe core-shell HNCs with different shell thickness. (b) Drawing of photoinduced charge separation and recombination between CdTe core and CdSe shell. (c) Plot of the time-resolved PL decay of CdTe cores and CdTe/CdSe core-shell HNCs with different shell thickness. Adapted with permission from ref. [43] Copyright 2010 The American Physical Society.

Time-resolved photoluminescence emission spectra of CdTe core and CdTe/CdSe HNCs shows that PL lifetimes increase as the shell grows. The radiative lifetime gradually increase from 15 ns (CdTe cores) to 38 ns (CdTe/CdSe),[10] demonstrating the formation of long-lived electron hole pairs as a result of a better charge separation in CdTe/CdSe type II system. In addition, the longer life-times indicate the suppression of non-radiative decay path obtained through the passivation of surface trap states of the CdTe core by CdSe

capping.[58,59] These peculiar characteristics, in addition to the extended near-infrared absorption, make type II HNCs suitable in photovoltaic applications, where light harvesting and charge recombination dynamics greatly influence the overall device efficiency.

2.3 HNC Quasi-type II

Quasi-type II regime exhibits a finite offset only for one carrier and a zero offset for the opposite one. Such an energy band alignment induces a delocalization of at least one carrier in the whole HNC.
Examples of quasi type II systems are CdS/ZnSe,[42] PbSe/CdSe,[61] PbSe/PbS[62] and CdSe/CdS.[45] It is worthwhile to mention that these systems are very sensitive to quantum confinement effects since variations in core or shell size can easily determine a transition from quasi-type II to type I or type II and vice versa. CdSe/CdS HNCs are usually referred as type I, but the small conduction band offset is not enough to distinctly confine electrons into the CdSe core. As a result, the electron wavefunction is delocalized over the entire HNCs, while the hole is confined in the core. The strong dependence between size and electron wavefunction localization have been investigated in CdSe/CdS dot-in-rod HNC configuration.[63]

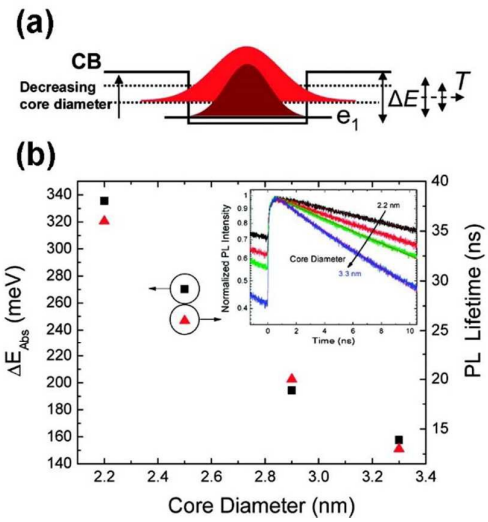

Figure 6. (a) Sketch illustrating the expected variation of conduction band configuration for different CdSe core diameters. (b) Energy variation ΔE for the first exciton absorption peak (black squares) between core-only and core/shell structures and the PL lifetime (red triangles) as a function of the core diameter. Time-resolved PL traces are shown in the inset. Adapted with permission from ref.[63] . Copyright 2011 American Chemical Society.

Figure 6 clearly shows the size dependence of radiative lifetimes of such HNCs. Dot-in-rod structures with smaller CdSe core, i. e. larger bandgap, show a longer exciton lifetime as a consequence of a high degree of electron delocalization.[63]Moreover, because of their large valence band offset holes remain confined into the core, regardless the core size and band-gap variation.

Similar behavior has been observed in quasi type II PbSe/PbS HNCs. In this case, the small valence band offset allows the delocalization of the holes over the entire HNCs, whereas electrons delocalization strongly depends on the core size (Figure 9).[62]

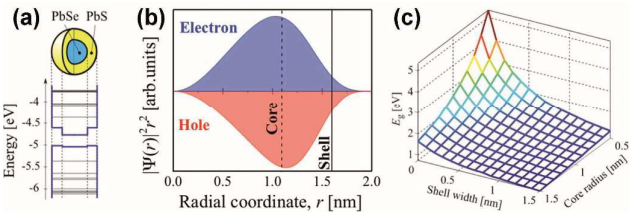

Figure 7. (a) Sketch of the PbSe/PbS core/shell structure (top) and a typical energy band diagram for 3.5 nm HNCs (bottom). (b) Calculated radial probability density of electron (blue) and hole (red) wavefunctions in PbSe/PbS core/shell HNCs. The core and the shell boundary are indicated with the vertical dashed and solid lines, respectively. (c) Dependence of the band gap energy on the core radius and shell thickness of PbSe/PbS HNCs. Adapted with permission from ref. [62]. Copyright 2014 American Chemical Society.

As consequence, in such HNC systems the optical band-gap varies with the core-to-shell ratio, and thus it can be tuned finely by simply increasing/decreasing the shell thickness. Furthermore, as in the case of CdSe/CdS HNCs, time resolved PL measurements reveal that PbSe/PbS HNCs exhibit a long radiative lifetime if compared to PbSe core only NCs.[62]

3. HNC based Light Emitting Diodes (LEDs)

Conventional inorganic semiconductor LEDs are efficient and stable but intrinsically point sources, requiring sophisticated processes for the integration in diffuse lightening sources. On the other hand, organic semiconductor technology has opened the possibility of fabricating diffuse and large-area light emitting panels by low-cost fabrication techniques, albeit with several limitations such as the short lifetimes at the high luminances (>1000cd/m^2) required for lightening application and different aging time, which varies for the diverse luminescent organic compounds. In this frame, the introduction of NC lumophores as active specie in LEDs could expedite the development of a facile and low temperature solution-based route to the assembly of devices via utilization of "inorganic inks" that combine the advantages of low-temperature solution-processable organic compounds, on one side, and the stable emission color of inorganic semiconductors.
The basic NC LED architecture consists of a stack of one or more NC layers, eventually combined with hole-transporting and/or electron transporting layers made of organic small molecule, semiconductor polymer, or metal oxide materials (i. e. ZnO), sandwiched between a transparent anode, usually indium tin oxide (ITO) and a metallic cathode (Figure 8).

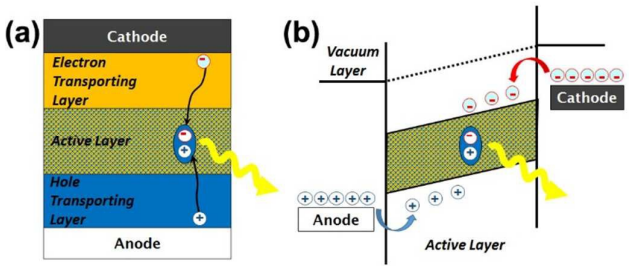

Figure 8. (a) Sketch of a general NC based LED structure and (b) a scheme of the basic operating principle.

When an appropriate voltage (typically between 2 and 10 Volts) is applied to the device, the injected positive and negative charges migrate within the thin film in opposite direction toward each other under the influence of the applied electric field. The excited state hole-electron pair is formed and it can emit light by radiative decay to the ground state, which competes with unwanted nonradiative recombination processes. The structure of the transport layers and the choice of the anode and cathode are designed to maximize the recombination process in the emissive layer.

The performance of LED devices can be characterized by its internal and external quantum efficiency (IQE, EQE), power efficiency or luminous efficacy (lm/W), luminous efficiency (cd/A), sometimes called luminous yield. The internal quantum efficiency is the number of photons generated inside the device per number of injected hole - electron pairs. The EQE is the number of photons released from the device per number of injected hole - electron pairs. The light out-coupling efficiency is determined by the refractive index of the emissive layer, and poor light extraction is one of the most important factor limiting the EQE of NC based and organic LED devices. Luminous efficacy is the ratio of the lumen output to the input electrical watts and the luminous efficiency measures the light output for a given current.

In NCs the radiative electron/hole recombination occurs in ns time scale[64,65] and competes with other deactivation mechanisms, such as phonon-assisted electron/hole and Auger recombination,[66] charge trapping at defect or dangling bond surface states.[65,67] In particular, the Auger recombination dominates the charge carrier dynamics in multiple electron-hole pair excitation regime, becoming very efficient in quantum-confined NC under electrically driven excitation since multiexciton generation can readily occur upon direct charge injection. Consequently, in the actual LED device,[68] the majority of NCs are prone to became dark and generate more heat than light. One of the most successful strategy to improve the surface quality and properties and to maximize the PL efficiency and, in turn, the LED performance, is the realization of expitaxially grown HNCs arranged in elaborate core/shell architectures.[69,70] Indeed, as discussed in the previous paragraph, having NCs a high surface/volume ratio, the presence surface states (vacancies, oxidation states, loss of passivating ligands, etc.) that can trap charge can strongly affect the optoelectronic quality of the material. Two design guidelines can be clearly identified for the chemical synthesis of high quality HNCs, amenable to LED application: the starting NC core needs to be monodisperse and the materials constituting the HNC should have minimal lattice mismatch.[71]

3.1 Effect of Shell Thickness and Crystalline Phase on hybrid LED Efficiency

In spherical NCs (QDs) the thickness of the inorganic shell can be increased (>5nm) to isolate the excited electron-hole pairs from the surface. This thick shell can be exploited to reduce the single-dot emission intermittency (blinking) phenomenon, strongly suppress non-radiative Auger recombination process[72] and increase the PL efficiency of HNCs.[73,74] Recently, to the aim of evaluating the effectiveness of this approach for hybrid LED application, a series of spherical CdSe/CdS HNCs with shell of increasing thickness have been synthesized and tested in the actual devices.[74] The CdS shell varied from 4 up to 16 monolayers, overcoating 3 nm diameter CdSe cores. As expected, the absorption and PL spectra shifted to lower energies when increasing the shell thickness. (Figure 9)

Albeit the PL efficiency measured in solution decreases by increasing the shell thickness, the corresponding LED devices for 11-16 monolayer outperform by more than an order of magnitude in EQE and luminance the thinner shell HNCs (4-8 monolayers). The authors attributed such an improvement to several cooperative effects discussed below. First, the optical properties of thick-shell HNCs are mostly independent of the passivating ligand coating, consequently the PL efficiency is likely to be retained in the films regardless the ligand degradation often occurring in solid state. In addition, the giant shell could reduce the probability of inter-NCs energy-transfer processes, which in densely packed NC films can lead to exciton diffusion and transfer to non-emissive trap states. Finally, the effective reduction of Auger recombination. Nonetheless, the performance of giant-shell based LEDs in terms of EQE and maximum luminance is not yet comparable to the best reported for hybrid inorganic–organic QD-LEDs.[68,75] These low performances has been ascribed to the spread size distribution and, therefore, an inhomogeneous broadening of the PL spectra and a poor ensemble PL efficiency of the giant core/shell HNCs.[73,76]

Besides the shell thickness, the design and synthesis of HNCs with an optoelectronic-grade for highly efficient LEDs requires the optimization of the crystalline quality of the material. To this purpose, Bawendi et al.[77] have developed successfully high-quality wurzite CdSe/CdS core/shell HNCs using cadmium oleate (Cd-oleate) and octanethiol as shell precursors. The low reactivity of octanethiol and strong carbonsulphur chemical bond favour a slow continuous shell precursor infusion keeping a narrow size distribution during shell growth. In addition, thanks to the small lattice mismatch (3.9%) between core and shell the resulting QDs maintain the CdSe core crystal structure. The single CdSe/CdS HNC blinking is effectively suppressed with a relatively thin shell (~2.4nm, corresponding to 7 monolayers) and the intrinsic ensemble PL is quite high.[77]

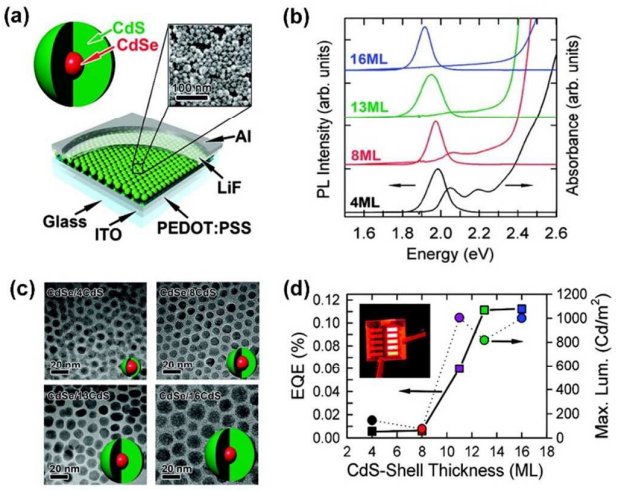

Figure 9. (a) A Scheme of the simple device architecture comprising the spherical CdSe/CdS HNCs, along with a sketch and transmission electron microscopy (TEM) image of HNCs. (b) Optical absorption and photoluminescence spectra of CdSe/CdS HNCs with increasing shell thickness: 4, 8, 13 and 16 monolayers. (c) TEM images of HNCs with different shell thicknesses. (d) EQE and maximum luminance vs CdS shell thickness graph. Inset: a photo of the working hybrid LED device. Adapted with permission from ref. [74]. Copyright 2012 American Chemical Society.

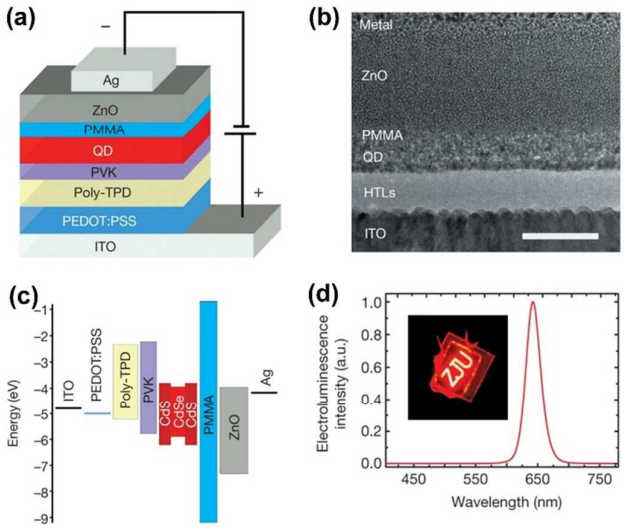

Figure 10. (a) A schematic of the hybrid LED device stack incorporating pure zinc blende CdSe/CdS core–shell HNCs. (b) TEM cross section of the device stack and (c) flat-band energy level alignment, the deep highest occupied molecular orbital of PVK facilitate the efficient hole injection. The insertion of a thin PMMA layer between ZnO and HNCs optimizes the charge balance in the device. (d) EL spectrum and a photo of the working LED device (inset) showing a saturated red emission. Adapted with permission from ref.[19]. Copyright 2014 Nature Publishing Group.

Lately, pure zinc blende CdSe/CdS core/shell HNCs have been synthesized with epitaxially grown shell, having a controlled thicknesses form 4 to 16 monolayers. This HNCs design allow obtaining non-blinking single NC emission and, most importantly, excellent reproducible optical properties at ensemble and PL efficiency >90%. Zinc-blend QDs were found to be substantially better in comparison to their wurtzite counterparts,[78] and this, according to theory,[79] have been attributed to a more symmetric crystal field of the zinc-blende structure, resulting in a less complex energy level landscape if compared to wurtzite. These zinc-blende HNCs with a shell of 10 monolayers were successfully integrated as active layer in solution-processed red emitting LEDs, with excellent performance and reproducibility.[19] The LED device architecture comprises staked layers of ITO anode, PEDOT:PSS, poly (N,N9-bis(4-butylphenyl)-N,N9-bis(phenyl)-benzidine) (poly-TPD, 30 nm), poly(9-vinlycarbazole) (PVK, 5 nm), CdSe–CdS core–shell HNCs (40 nm), poly (methylmethacrylate) (PMMA, 6 nm) ZnO nanoparticles (150 nm) and silver cathode (Figure 10). The insertion of the thin insulating PMMA polymer between the HNCs and ZnO transporting layers allows optimizing the electron-hole charge balance in the device, modulating the injection in the active layer and to preserve the HNC emission properties, which could be degraded by an excess of charge accumulation. Notably, such devices represent the best-performing solution-processed red LED so far, showing superior external quantum efficiency of 20.5%, low efficiency roll-off and a turn-on voltage of 1.7 V, combined with a good stability of more than 100,000 hours at 100 cd/m^2.[19]

Following the same concept, zinc blende CdSe cores have been used as seeds to grow onion like high quality CdSe/CdS/ZnS HNCs. LED devices with emission in the green and orange portion of the visible spectra have been successfully demonstrated with current efficiencies of 16.4 cd/A for the green and 12cd/A for the orange emission.[80]

In addition to visible-emitting devices, the core/shell heterostructuring strategy has been used to improve the performance of hybrid infrared LEDs. High-performance shortwave-infrared LEDs have been recently fabricated by using PbS/CdS QDs as emitting species.[81] Such devices show a maximum external quantum efficiency up to 4.3% ± 0.3% that is by 50-100 fold improvement if compared to the PbS core only based devices. The turn voltages are lowered by 0.6 ± 0.2 V and per-amp radiant intensities are increased by up to 150 times. The authors proposed that such a performance enhancement are due to the passivation of PbS cores by CdS shells. Further demonstrating the potentiality of HNCs for NCs application in LEDs.

3.2 Alloyed-shell growth: improved structural uniformity and LED efficiency

A second approach to limit the undesired Auger process, and consequently to improve the efficiency of HNC based LEDs, is to reduce the confinement potential by the stepwise change in lattice parameters. This strategy allow improving the structural uniformity in shell growth and reducing the interfacial core/shell defects, which are likely to occur at a steep interface between different materials because of the lattice stress.[47] The gradual chemical compositional gradient enables effective strain relief, thus improving the optical properties of the resulting HNCs. The composition gradient in the intermediate shell can be adjusted by varying the relative ratios of the precursors.

This concept have been exploited to develop HNC QDs with a graded, alloyed intermediate shell ($Cd_{1-x}Zn_xSe_{1-y}S_y$) sandwiched between the Cd- and Se-rich core and the Zn- and S- rich outer shell. The amounts of Zn and S are modulated to tune the composition of the intermediate shell, obtaining either Cd- and S-rich or Zn- and Se-rich intermediate shell (named as CdS-rich and ZnSe- rich HNCs). Blue, green and red LEDs with high external quantum efficiencies (14.5% for green, 12.0% for red and 10.7% for blue devices) have been reported by this approach, demonstrating that the fine compositional design could have a preeminent role in determining the final LED performances thanks to its beneficial effect on charge injection, transport and recombination.[8]

The sketch of the solution processed device multilayer incorporating graded ZnCdS/ZnS HNCs is reported in Figure 11 a-b, and consists of conventional sandwiched devices architecture with the addition of a poly(9,9-dioctylfluorene-co-N-(4butylphenyl)diphenylamine) (TFB) and ZnO nanoparticle hole transport and blocking layer respectively. The ZnO layer allows for efficient electron injection along with a good confinement of holes into the HNC active layer, ensuring high emissive charge recombination efficiency.[82] In addition, the ZnO nanoparticles act as a protective barrier for moisture, and could improve the device stability. All the graded HNCs based LEDs are fabricated by solution processing amenable to mass production, with a low turn-on voltages and saturated pure color emission. Notably, green and red LEDs are quite stable showing a lifetime of 90,000 and 300,000 h.[8]

The alloyed-shell shell concept and the same device configuration have been recently exploited for the fabrication low turn-on voltage blue-violet LEDs[83] (Figure 11 c-d). By analogy with organic small molecule, obtaining color saturated blue emission at high performance is an open issue in NC based LEDs. The difficulties resides in the wide band gaps required for pure blue emission, which obstacles the efficient hole and electron injection in the active layer, and the increased energy loss pathways for exciton quenching. For these reasons, the EQE of blue NC based LEDs is still lower than those of the best performing red and green emitting ones,[80,84–87] with a high turn on voltage>3 V that lowers the luminous power efficiency and reduces the device operation lifetime. High efficiency blue-violet devices have been realized by using the graded shell ZnCdS/ZnS HNCs as active emitting species. Such HNCs show a uniform size distribution, continuous composition gradient with small lattice mismatch (<6.8%) between ZnCdS and ZnS.

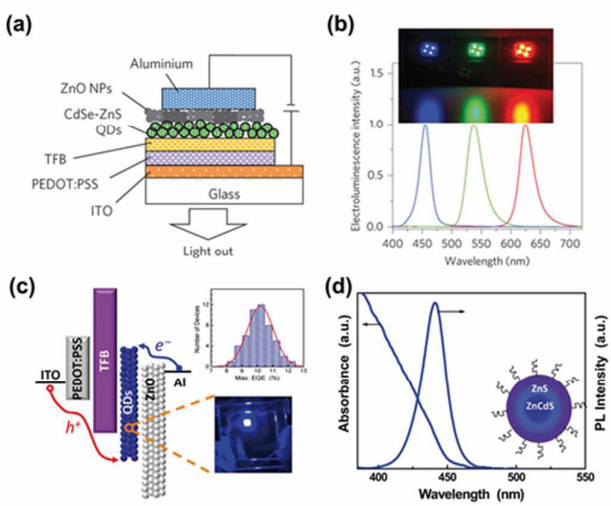

Figure 11. (a) A sketch of the ZnCdS/ZnS HNC based device. (b) EL spectrum and a photograph of the blue, green and red emitting LEDs. Adapted with permission from ref. [8] Copyright 2015 Nature Publishing Group. (c) A scheme of the energy level diagram, along with a photo and a maximum EQE value distribution of the blue emitting LED based on graded shell ZnCdS/ZnS HNCs. (d) PL and absorption spectra of the and a sketch of the spherical ZnCdS/ZnS HNCs. Adapted with permission from ref. [83]. Copyright 2015 American Chemical Society.

Most notably, these HNCs are characterized by excellent optical properties, such high PL quantum yield of about 90% in solution, pure and deep-blue light (peak at 441 nm) with narrow spectral breadth (~20nm), and non-blinking effect. In order to improve the device efficiencies by balancing the electron/hole current, the HNCs undergo ligand exchange process that substitute the long and insulating native oleic acid ligand with shorter 1-octanethiol. The turn-on voltage (~ 2.3 V) is lower than the photon voltage of the HNC optical band gap (hν = 2.8 eV), and is attributed by the authors to the Auger-assisted energy upconversion process trigged by the ZnO nanoparticles layer.[52,83] A maximum luminance of L = 5,700 cd/m^2 is achieved at 5.5V and a peak EQE of 6.7% and current efficiency of 1.3 cd/A.

Graded shell concept has successfully applied in an onion-like multishell CdSe/CdS/ZnS HNCs. Thanks to the low lattice mismatch, and consequently high PL efficiency (up to 85%), CdSe/CdS/ZnS QDs has led to good performances for LED applications.[13,53,88]

A similar approach has been used to improve the shell thickness and passivation on Cd-free InP QDs. For LED application, mitigation of environmental concerns related to nanocrystalline materials relies on the replacing of toxic Cd heavy metal element.[89] InP NCs[90] is regarded as the most promising for a possible substitution of Cd-based II-VI compounds. Albeit considerable progresses in the synthesis of InP based materials, the optoelectronic properties and stability of Cd base HNCs are still superior. Such a gap is mainly attributed to the difficulties in controlling the reaction process, caused by covalent bonding character and difficulties in obtaining an optimum surface passivation. Among available materials, ZnSe is regarded as the best choice for InP-based

NCs, thanks to the low toxicity and a sufficient lattice parameter fitting. However, the lattice mismatch between the InP core and higher band-gap ZnS shell is still too high leading to compressive lattice strain, limiting the maximum thicknesses of the shell to be <1 nm, hindering the environmental stability of InP HNCs.

Growing a graded ZnSe/ZnS shell in the radial direction has been demonstrate to be a successful strategy to synthesize InP HNCs: the ZnSe alleviates the lattice strain while the ZnS protect the HNCs from degradation. Carrier localization in these HNCs is a quasi type-II regime, while hole wave functions are mostly confined in the InP core phase, electron wave functions are delocalized to the shell phase. Such a stratagem allows obtaining InP/ZnSeS core/shell QDs with high PL yield and stability.[91–93] The PL yield greatly enhances upon the shell growth and increasing the shell thickness up to > 70% with ~6 monolayers of ZnSeS. (Figure 12a-b) To date this InP/ZnSeS multishells material PL yield has led to the best performing LED based on Cd-free HNC materials.[93]

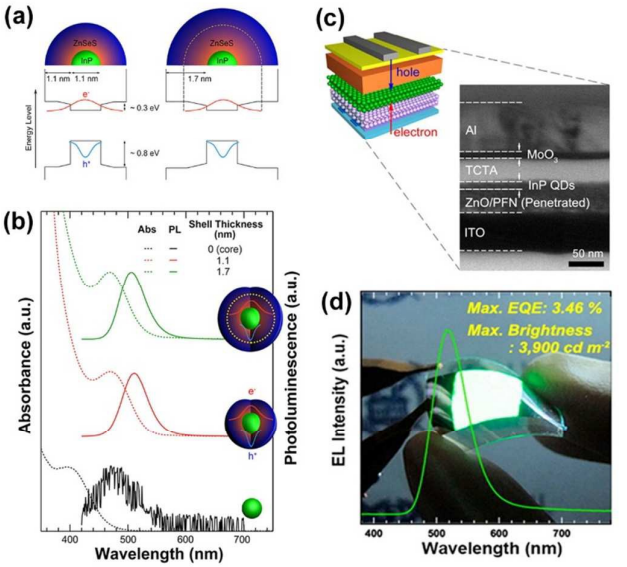

Figure 12. (a) Energy level diagram and InP/ZnSeS multishell HNC sketch with 1.1 nm and 1.7 nm shell thickness. (b) Absorption and PL spectra of InP core only (black), InP/ZnSeS HNCs with 1.1 nm (red) and 1.7 nm (green) shell thicknesses. (c) A schematic of the hybrid LED device stack along with a TEM cross section. (d) EL spectra and a photo of the working LED device. Adapted with permission from ref. [93] Copyright 2013 American Chemical Society."

This breakthrough in device performances is achieved by engineering the device architecture for direct charge carrier injection into InP/ZnSeS HNC with the aim of improving the exciton recombination. The direct electron injection within HNCs is obtained by a solution-processed thin conjugated polyelectrolyte layer (poly[(9,9-bis(30-(N,Ndimethylamino) propyl)-2,7-fluorene)-alt-2,7-(9,9-ioctylfluorene) (PFN), such a PFN layer acts as an interfacial dipole layer between the ZnO electron transport layer and HNCs, reducing the electron injection barrier and promotes the charge balance within HNCs (Figure 11c). The resulting LEDs show a record external quantum efficiency of 3.46% and a luminance of 3900 cd/m^2, representing 10-fold increase in device efficiency compared with previous reports on the same Cd-free material. (Figure 11d)

A similar approach to efficiently passivate the surface defects of InP cores, is the "strain-relieved" growth. This method consist in synthesizing the InP cores in a Zn-rich environment, zinc carboxylates, which leads to a surface stabilization of the InP/ZnS core/shell HNCs.[94] The high-quality InP/ZnS HNCs with a high PL quantum yield of ~60%, narrow emission linewidth and good photostability were obtained. White emitting hybrid LED based on the resulting InP/ZnS HNCs has been successfully demonstrated.

It is worth mentioning that other HNCs, albeit with poorer efficiency, have been synthesizes for the developed of Cd-free LEDs. As an example, Cu-doped InP/ZnS/InP/ZnS shell QDs with a double band emission,[95] multishell HNCs InP,[96] and ZnSe based QDs have been reported.[97] All these works demonstrate that the preparation of efficient and stable Cd-free materials for the future implementation in LED technology are feasible.

3.3 Tuning the Confinement Regime through Shape-Design of HNCs.

Multi-color emission in HNC LEDs is usually obtained by an accurate selection and mixing of colloidal NCs with different sizes. To obtain white light, all the three primary colors (red, green and blue) have to be produced simultaneously.[14] As an example, white bright emission EL has been obtained from homogenous blends, without phase segregation between the active ternary of CdSe/ZnS HNCs composites and the organic matrix 4,4,N,N-diphenylcarbazole (CBP), exploiting the energy transfer and charge-trapping properties of the different species.[98] In another approach contact printing has been exploited to deposit HNCs atop of a p-doped organic layer.[99] Recently, an alternative HNC "dot-in-bulk" configuration has been proposed to obtain two-color emitting material under optical and electrical excitation. In the "dot-in-bulk" NHSs, the quantum confined CdSe core is surrounded by a 7-9nm bulk-like CdS shell (Figure 13).[100,101]

The emission color of such HNCs is a combination of the core and shell emission band and, could be modulated by the intensity of the optical excitation (for PL) or the applied bias in electroluminescent devices. Generally, in conventional CdSe/CdS core/shell HNCs the large valence band offset from one side and the small conduction band offset from the other lead to the formation of a quasi-type II heterojuntion. This configuration leads to strong confinement of holes in the core and delocalized electrons in the entire HNCs, and due to the fast hole relaxation,[102] the emission occurs by radiative recombination of the core exciton. The design of the "dot-in-bulk" HNCs allows to slower the relaxation time of holes in the core and that holes can possibly recombine in the bulk like CdS shell, resulting in a double peak emission. The LED device consist of a sandwiched like architecture, in which the HNC layer is solution deposited onto PEDOT:PSS hole injection layer, and the LiF/Al cathode is thermally evaporated. The device shows a dual color emission, resulting in overall yellow light with a luminance of 2000cd/m^2 and efficiency of 0.1%, which can be tuned by changing the applied bias.[101]

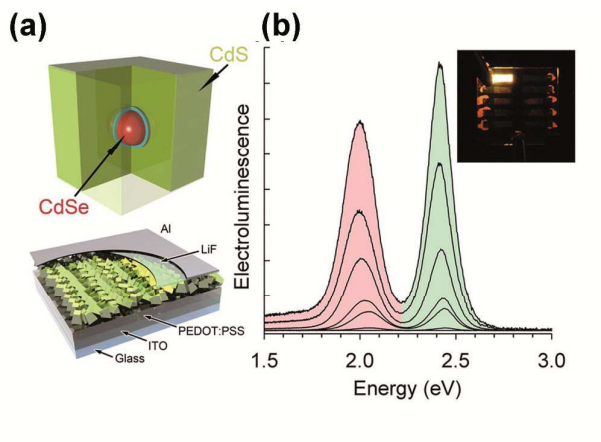

Figure 13. (a) Illustration of a "dot-in-bulk" HNC and device LED architecture. (b) Dual-color EL spectra HNC based LED along with a photo of the working device. Reprinted with permission from ref. [101]. Copyright 2014 American Chemical Society.

Dual emissive peaks under single-excitation wavelength are obtained in a type-II core–shell system consisting of Cu-doped CdS core–ZnSe shell NCs, by superposition of core and shell emission.[103] The emission is tuned in the wavelength range from visible to near-infrared by simply controlling of the doping of CdS and the shell thickness, respectively. Such engineered HNCs exhibit characteristic ''zero self-absorption,'' but also show high quantum yield (56%) and good thermal stability. White LED lamp was fabricated using a commercial blue LED chip combined with the Cu-doped CdS-ZnSe as color converters.

Alternatively, localization of electron/hole wavefunction and PL quantum yield can be tuned by synthesizing elongated core/shell HNCs. Synthetic developments based on the seeded-growth approach[104] have yielded CdSe/CdS core/shell-type nanorods with narrow distributions of both lengths and diameters, which additionally emit wavelength-tunable, linearly polarized light with high efficiency. The seeded-growth is performed by co-injecting appropriate precursors and preformed spherical CdSe monodisperse QD seeds in a mixture of hot surfactants suited for the anisotropic growth of CdS HNCs. The presence of the seeds allows bypassing the homogeneous nucleation and finally obtaining a narrow size distribution. Varying the aspect ratio (rod length/rod diameter) of the nanorod HNCs, the PL quantum yield increases up to 70-75% (aspect ratio of 3) and decrease to 10% for longer nanorods (aspect ratio 28). In general, for aspect ratio larger than 10, the decrease in PL efficiency can be due a more delocalized electron wave function together with an increasing number of surface trap states arising from the CdS region.

Thanks to their regular shape and permanent dipole moment along the long axis due to the noncentrosymmetric wurtzite lattice structure,[105,106] such rod shape HNCs are prone to self-assemble into ordered anisotropic solids, which has recently been exploited to realize LED with polarized emission (Figure 14a-b).[107] Close-packed films of ordered HNC rod arrays are obtained by spreading onto a water surface a drop colloidal nanorod, which during the solvent evaporation spontaneously self-assemble in an ordered film at the water/air interface. Subsequently, a poly(dimethylsiloxane) PDMS stamp pad is used to fish and transfer by contact printing the close-packed film from the water surface to a previously evaporated organic thin film, which acts as hole transporting layer for the actual device. The hybrid LEDs has been fabricated in a multilayer organic/inorganic device architecture, consisting of a thermally evaporated N,N'-bis(naphthalen-1-yl)-N,N'-bis(phenyl)benzidine (α-NPD) hole injection layer doped with 2,3,5,6-tetrafluoro-7,7,8,8-tetracyanoquinodimethane (F4-TCNQ) and a CBP hole transporting layer. The HNC rod film acts as the emissive species, and the device is completed with thermally evaporated 3-(4-biphenylyl)-4-phenyl-5-t-butylphenyl-1,2,4-triazole (TAZ) hole blocking layer, tris(8-(hydroxyl-quinoline) aluminum (Alq_3) electron transporting layer, and LiF/Al electrodes.

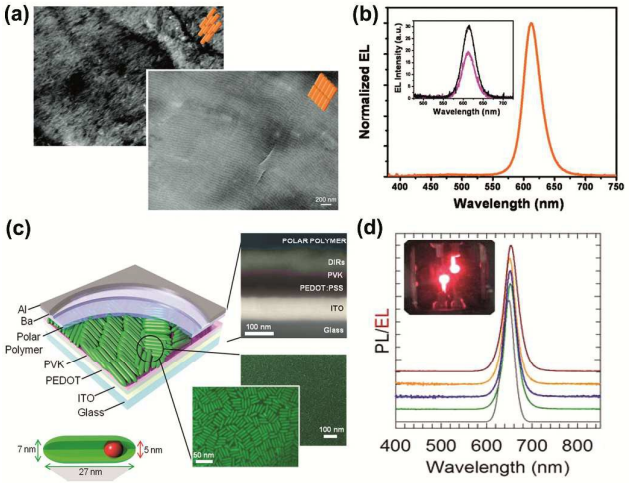

Figure 14. (a) Scanning electron microscopy (SEM) images of nanorod shaped HNC s arranged in smectic/nematic. (b) Normalized EL spectrum of the nanorod HNC based LEDs. Inset: EL spectra for two orthogonal direction, showing polarized emission. Reprinted with permission from ref. [107]. Copyright 2009 American Chemical Society. (c) A sketch of the nanorod based LED, along with a (b) SEM cross section of the device structure and SEM images of the active and transporting layers. (d) PL and EL HNC emission and a photo of the working LED device. Adapted with permission from ref. [108]. Copyright 2015 American Chemical Society.

In the proposed structure the holes injection has been improved by p-doping the α-NPD matrix with the strong electron acceptor F4-TCNQ. The F4-TCNQ molecules remove electrons from the α-NPD highest occupied molecular orbital states and hence generate holes. Moreover, the use of a TAZ avoids the transfer of holes and excitons into the Alq_3 and consequently inhibits the emission from this layer. The maximum brightness of 170 cd/m^2 was reached at 19 V and at 140 mA/cm^2, and the maximum current efficiency of 0.24 cd/A was reached at 12 V. The electroluminescence spectra for two orthogonal polarization directions, showing polarized light emission, are reported in the Figure 14a-b along with the scanning

electron microscopy images of the HNCs rods aligned in either smectic or nematic fashion.

Very recently, similar rod shaped CdSe/CdS HNCs have been integrated in a solution based processed bright and efficient red emitting LEDs.[108] The device architecture in depicted in Figure 14c-d, the HNC rod films is sandwiched between PEDOT:PSS/PVK hole injection/transporting layers and a polyelectrolytic electron transporting layer with mobile Br- counteranions. Most notably, the device has low turn-on voltage of ~ 3 V, high brightness of 1200 cd/m^2, and external quantum efficiency of 6.1% with no roll-off at high current densities that the authors attribute to the use of the polyelectrolytic electron transporting layer.

The best performing LEDs based on elongated HNCs have been prepared starting from double-heterojunction nanorods consisting of seed CdS nanorod with an average 27.6nm length and 4.1nm diameter with CdSe grown at the tips and a ~0.7 nm ZnSe shell overcoating the CdSe tips (Figure 15).[109,110]

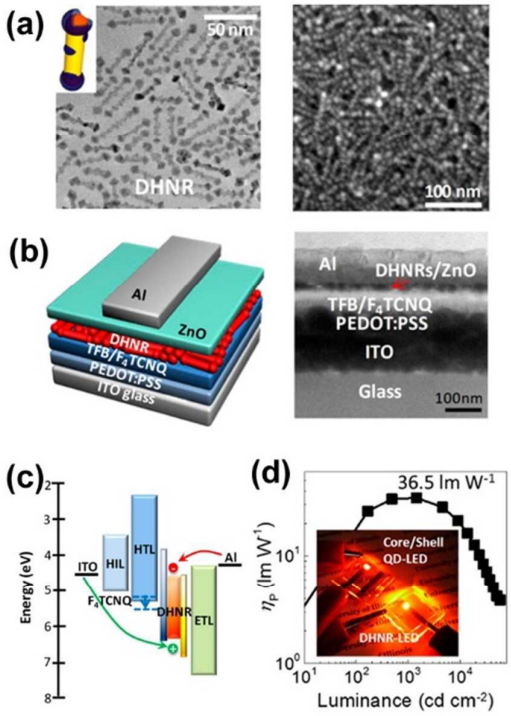

Figure 15. (a) TEM and SEM images of double heterojunction nanorod HNCs. Inset: an illustration of the CdS nanorods with the ZnSe/CdSe tips. (b) Schematic and TEM cross-section of the hybrid LED structure and (c) energy level alignment. (d) Power efficiency and a photo of the working LED device. Adapted with permission from ref. [110]. Copyright 2015 American Chemical Society.

The double heterojunction nanorods form a type II staggered band alignment and are both in contact with one smaller band gap material. Such a configuration provides independent control over the electron and hole injection/ extraction processes keeping high photoluminescence quantum yields (~40%) and narrow linewidth.

Record efficiency has been obtained by integrating such HNCs into optimized device geometry, which is schematized in Figure 14b-d. The hole transporting layer consist of poly[(9,9-dioctylfluorenyl-2,7-diyl)-co-(4,40-(N-(4-sbutylphenyl)) diphenylamine)] (TFB) doped with the strong electron acceptor F4TCNQ. The introduction of F4TCNQ dopant improves the hole injection/transport and makes the TFB more resistant to solvent for the subsequent deposition of the HNC layer. ZnO nanoparticles are used as electron transporting materials. The band alignment of the different layers in the device stack allow obtaining exceptional performances thanks to optimized carrier injection, minimized energy transfer losses and enhanced light outcoupling. The LEDs based on such double heterojunction nanorod HNCs feature a maximum brightness of 76000 cd/m^2, a current efficiency of 27.5 cd/A, a power efficiency of 34.6 lm/W and an external quantum efficiency of 12%.

Another innovative and intriguing approach to obtain high PL efficiency, is the design of quasi-2D colloidal nanoplatelet HNCs. Core/shell CdSe/CdS and CdSe/CdZnS semiconductor atomically thin nanoplatelets have been recently demonstrated.[111] Such HNCs have been obtained by starting from CdSe nanoplatelets and growing a shell by using a layer-by-layer process, which allows obtaining a precise control over the shell thickness resulting in a homogeneous 2-nm-thick shell. Such 2D HNC have been then tested as active material in a hybrid LED configuration in which organic PVK polymer and ZnO layers acting as charge transport layers and optical spacers.[112] These LEDs a maximum EQE of 0.63% coupled with narrow spectral breadth (25–30 nm), which is characteristic of the 2D nanoplatelet HNCs. The present result open the avenue for the synthesis of a new class of material with excellent color purity.

4. HNC application in photovoltaic devices

The basic working principle of colloidal NCs-based solar cells involves several physical steps: (i) light absorption and electron-hole pair (exciton) generation, (ii) exciton dissociation and (iii) charge carriers collection to the electrodes (Figure 16a-b).

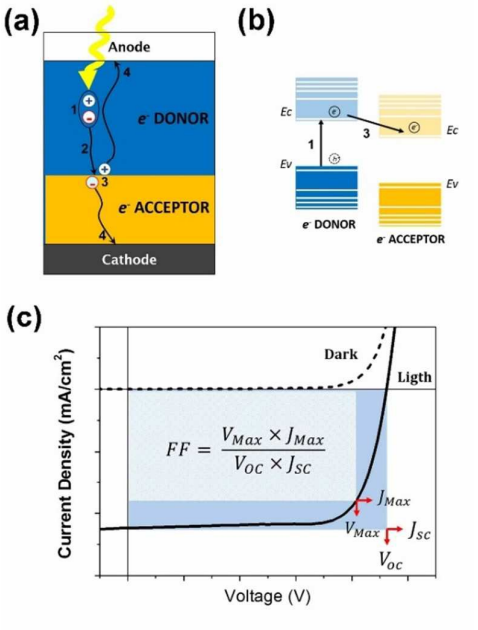

Figure 16. (a) Sketch illustrating the physical steps involved in the generation of photocurrent: (1) light absorption and

exciton generation, (2) exciton diffusion, (3) exciton dissociation at the interface between donor and acceptor materials (4) charge carriers collection to the elctrode. (b) Energy band alignment between donor and acceptor materials. (c) Typical J-V curve of a solar cell showing the Voc, Jsc and the FF. Vmax and Jmax represent the voltage and current density at maximum output power density.

In general, the overall power conversion efficiency (PCE) of the photovoltaic devices is the product of three key parameters: the open circuit voltage (Voc), the short circuit photocurrent density (Jsc), and the fill factor (FF), which represent the ratio between the maximum output power density of the device to the product of Voc and Jsc (Figure15c).
In order to maximize device efficiency, each of these three factors - Voc, Jsc, and FF - need to be optimized by engineering the device architecture and the photoactive material absorption properties. Using semiconductor NCs as active material in photovoltaic devices has several advantages if compared to the organic semiconductor counterparts. NCs typically exhibit much larger extinction coefficients over a broader spectral range, allowing for a better matching of solar radiation and an improved light harvesting capability, which could rise the photocurrent generation when integrated in an actual device. The NC material selection guides the band-gap tuning, as an example Cd based NCs can harvest the entire visible spectral range,[113] and complementary, smaller band-gap Pb chalcogenide NC materials can be used to cover the infrared region of solar spectrum.[114] However, the use of too low band-gap materials would lower the Voc and, being the cell's power output the product of Jsc and Voc, band-gap in the range of 1.1 and 1.4 eV represent a good tradeoff to maximize device performance.
In this section, we will discuss the recent advances in creating functional HNCs and the possible impact on the development of next generation low-cost and high-efficiency solar cells.

4.1 Effect of Shell Thickness on solar cell efficiency and photo-stability

PbS or PbSe semiconductors are among the most promising materials for NC based photovoltaic devices thanks to their extended absorption spectra in the near infrared region[114] as well as to the possibility of hot carrier extraction[115] and multiple exciton generation.[116] A successful example of Pb based HNCs applied to solar cells is type I PbS/CdS QDs. PbS/CdS HNCs have been used as p- type layer in a p-n heterojunction device in which the n-type layer consists of colloidal ZnO nanoparticles. In type I HNCs usually the shell exhibit an energy band gap wider than the core one. The resulting core-to-shell energy band offset confines both charge carriers, electrons and holes, into the core of the HNCs. Albeit the shell could potentially act as an energy barrier for charge carrier extraction, it plays a fundamental role in obtaining an efficient passivation of dangling bonds, thus enhancing material photostability and, potentially, improving device performance. It has been reported that minimizing the shell thickness, limiting the barrier effect, charges can be still easily extracted from the core of type I HNCs.[117–119] Therefore, through intelligent shell thickness engineering, NC stability can be greatly enhanced without affecting charge carrier extraction and transfer dynamics. PbS/CdS QDs are synthesized through a low-temperature cation-exchange method[51] that, thanks to the low working temperature, minimizes the Ostwald ripening effect and leads to narrow NCs size distribution. Moreover, by using the cation exchange technique the CdS shell grows at expense of the PbS core which decreases in size during the shell formation. The reduction in PbS core diameter impacts on the optoelectronic properties of PbSe/PbS HNCs leading to a blueshift in the excitonic peak associated to the widening of the PbS core bandgap. Consequently, Voc value could positively be affected from both the reduction of surface traps and the wider bandgap of PbSe/PbS HNCs. When integrated in the actual devices, PbS/CdS HNCs leads to an increased Voc value of more than 0.2 V, if compared to the PbS core only.[21,120] The authors demonstrate that the density of trap state is reduced in the HNCs thanks to an efficient surface passivation through the CdS shell and the emission decay lifetime is increased, due to the suppression of non-radiative recombination channels. It is worth to note that too thick CdS shells (> 0.1 nm) act as a tunneling barrier to charge transfer between each single HNCs, which is detrimental for the device efficiency.[21] Further surface treatments on PbS/CdS HNCs films, by using halide and dithiol ligands, could increase carrier mobility and thus they maximize device performances. Using this approach, the best device performances including PbS/CdS HNCs are achieved with a CdS shell thickness of 0.1 nm and by performing a combined surface treatment with cetyltrimethylammonium bromide, as bromine source, and ethane dithiol. In this latter case a PCE of 6.05%, a FF of 0.39, Voc 0.65 V and current density of 23.9 mA/cm^2 have been reached (Figure 17).[21] These results demonstrate that the 0.1 nm shell thickness represent an optimal compromise that ensures at the same time both an efficient defect state passivation and charge extraction.

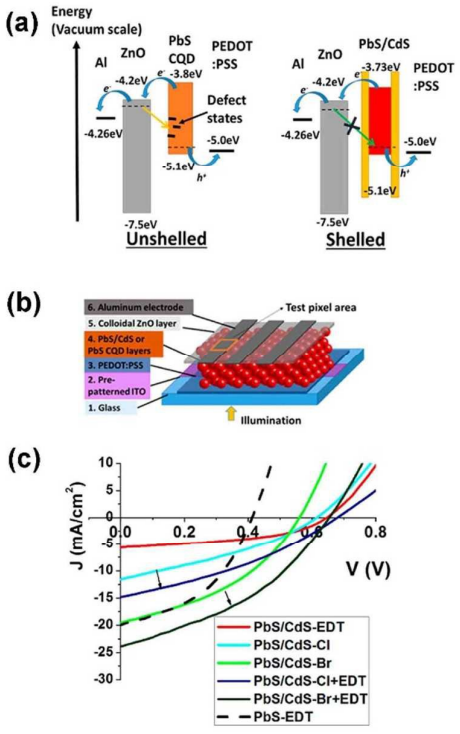

Figure 17. (a) Schematic Energy band alignment of the heterojunction cell and the effect of a CdS shell on the PbS electronic structure. Defect states in the unshelled PbS NCs

promotes non-radiative recombination, whereas the addition 0of a CdS shell reduces recombination and thus improve Voc values. (b) Drawing of the device architecture used for performance testing. (c) Current-to-Voltage curves of the PbS and PbS/CdS HNCs based devices obtained performing different ligand exchange treatments on NCs films. Adapted with permission from ref. [21] Copyright 2014 American Chemical Society.

In addition, PbS/CdS HNCs have been exploited in quantum dot sensitized solar cells as light harvesting material, in which HNCs are directly absorbed on mesoporous TiO_2 instead of conventional dye molecules.[121] The CdS shell increases the electron lifetime into the PbS core leading to an enhancement of the electron diffusion length and charge collection. Also in sensitized solar cells, thicker CdS shell acts as an energy barrier to charge injection to the electrodes. The best results have been achieved using PbS core with a shell of CdS of 0.5 nm, with a PCE of 1.18%, a Jsc of 5.70 mA/cm^2, a Voc of 0.47 V and a FF of 0.44, whose values are significantly higher than that obtained with PbS core-only NCs.

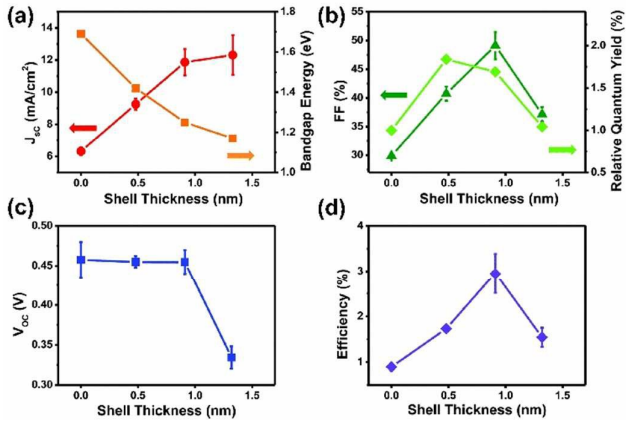

Figure 18. PbSe/PbS based solar cell characteristics (a) Variation of J_{SC} (red circles) with effective band gap energy (orange squares), (b) FF (green triangles) with relative quantum yield (pale green diamonds), (c) V_{OC}, and (d) power conversion efficiency depending on the PbS shell thickness of 0.5, 0.9, and 1.3 nm. Adapted with permission from ref. [9] Copyright 2015 The Royal Society of Chemistry.

The best performing sensitized solar cells has been reported by including spherical ZnTe/CdSe Type II HNCs.[122] In particular, by using ZnTe/CdSe HNCs as sensitizers, electrons localized in the CdSe shell are rapidly injected in the TiO_2 electrode while the holes remain located in the ZnTe core. This leads to the creation of a dipole moment that upshifts the conduction band edge of the TiO_2. As a result, solar cells sensitized with ZnTe/CdSe HNCs exhibit an improved Voc that allows to reach a PCE of 6.82% which is higher than CdSe core only NCs sensitized solar cells (PCE= 5.33%).[122]

Recently, quasi-type II PbSe/PbS HNCs have been synthetized and integrated in solar cell devices. In general, in quasi type II HNCs the conduction or the valence band offset is extremely small, and holes are usually delocalized over the entire core/shell structure, whereas the degree of electron delocalization depends on the size of the HNCs.[62] In the particular case of small size PbSe/PbS HNCs, both electron and hole are delocalized over the all HNC volume. In this case, charge carrier separation, extraction and transport is improved and this is extremely favorable for photovoltaic applications, as it has been demonstrated by integrating PbSe/PbS HNCs that showed an higher PCE if compared to non-shelled PbSe NCs.[9,123]

In details, the increase of the PbS shell thickness turned out to be in a 95% increment of the Jsc because of the enhanced light harvesting due to the shrinking of the bandgap.[9] Furthermore, the PbS shell has the advantage of reducing the charge trap density of the PbSe core and thus it leads to an increases FF thanks to the reduction of trap assisted recombination phenomena. The reduction of surface traps is also beneficial for the Voc, whose value does not change despite the band-gap reduction. However, shells thicker than 1nm lead to a drastic decrease of the overall device efficiency. (Figure 18) This are ascribed to the formation of recombination centers during the thick shell growth possibly caused by lattice strain. However, as in the case of PbS/CdS HNCs, further halide treatment are required to provide higher carrier mobility and longer diffusion length in the HNCs solar cells, which leads to improvement in the solar cell performance. At present, the best device performance are reached with PbSe/PbS HNCs having a shell of 0.9 nm thick. The best device exhibits a Jsc of 21.7 mA/cm^2, a Voc of 0.5 V, a FF of 57% and PCE of 6.5%.[9] Therefore, further efforts are necessary for the development of new synthesis protocols for high-quality thick-shell PbSe/PbS HNCs.

4.2 Improved Charge Percolation through Shape-Design of HNCs.

With the aim of improving the charge separation efficiency, type II CdTe/CdSe HNCs with branched tetrapod shape have been conceived.[124] In principle, in Type II HNCs the staggered band alignment leads to ultrafast photoinduced charge separation and increased charge carrier lifetime. Moreover, Type II HNCs could exhibit also better light harvesting properties due to the contribution from both the two material components and from charge transfer states that exist at the interface between the two semiconductors. Such features make type II HNCs an appealing material for photovoltaic applications.

Despite the efficient charge separation at the interface between CdTe and CdSe in addition to the advantageous tetrapod shape of the HNCs, the performance of such devices is limited by the inefficient charge extraction from the HNCs and by the lack of a continuous charge percolation path to the electrode. To overcome this problem, type II CdSe/CdTe tetrapods have been used in a double layer photovoltaic device structure, together with a 40 nm thick C60 layer. The C60 layer allows an efficient electron extraction from the CdSe core, due to its favorable energy level alignment with CdSe, besides to be characterized by a high electron mobility. Such hybrid device leads to a PCE of 0.6%, a Jsc of 3.15 mA/cm^2, a Voc of 0.43 V and a FF of 0.46 (Figure 19).[125]

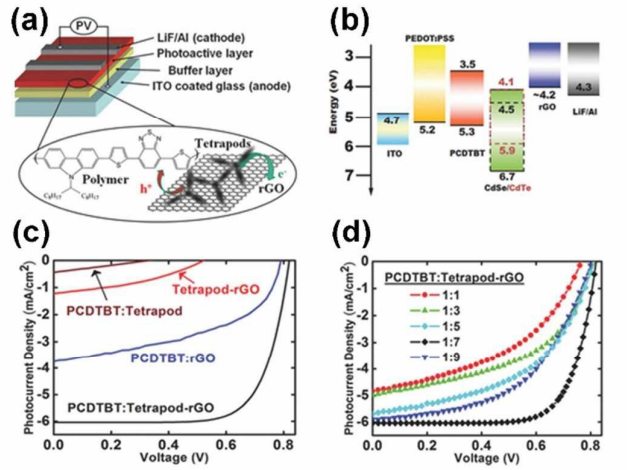

Figure 19. (a) Photovoltaic device configuration including PCDTBT: CdSe/CdTe tetrapods-rGO nanocomposite. (b) Schematic energy level alignment of the device. J-V curves of the devices with (c) different photoactive layer and (f) PCDTBT:Tetrapod-rGO in various blend ratio. Adapted with permission from ref.[126] Copyright 2013 Wiley-VCH.

Further improvements in type II CdSe/CdTe tetrapods based solar cells have been reached by linking tetrapods with conductive reduced graphene oxide sheets (rGO) before blending it with Poly[[9-(1-octylnonyl)-9H-carbazole-2,7-diyl]-2,5-thiophenediyl-2,1,3-benzothiadiazole-4,7-diyl-2,5-thiophenediyl] (PCDTBT).[126] In such hybrid systems, the simultaneous presence of rGO and PCDTBT ensure an efficient electron/hole separation and transport, leading to an enhancement of the overall device performances. Devices including PCDTBT:tetrapods-rGO blend are characterized by an high Voc of 0.82V, a Jsc of 6.04 mA/cm^2, a FF of 0.5, which it yields to a PCE of 3.3%, that is significantly higher than that reported results without rGO. The high photovoltaic performances obtained with PCDTBT:tetrapods-rGO nanocomposite demonstrate that, for an efficient exploitation of type II HNCs, electron and hole extraction/transporting materials are essential.

5. Conclusions and Outlook

Surfactant assisted colloidal synthesis of epitaxially grown HNCs opens the route for the fabrication of efficient and innovative LEDs and solar cell devices.

Recent advances in the field have led to the realization of HNCs based on several semiconductor materials combined into complex onion like core/shell, dot-in-rod, and branched structures. In addition, the heterostructuring framework allows modulating the hole and electron wavefunctions, thus modifying the carrier confinement regime. Such an approach offers the undoubted advantage of construct various shapes, combination of semiconductors, graded or net core/shell interfaces finally providing a facile and unprecedented control over the photo-physical and optoelectronic properties of HNCs.

Concerning LED application nano-heterostructing strategy has led to the demonstration of highly efficient and multi-color devices. A proper shell thickness optimization has been demonstrated to reduce blinking phenomenon and strongly suppress non-radiative Auger recombination process, thus increasing the PL efficiency of HNCs.

Besides the shell thickness, highly efficient LEDs requires the optimization of the crystalline quality of the two adjoined materials. The best performing solution-processed red LED, showing superior external quantum efficiency of 20.5%, low efficiency roll-off and a turn-on voltage of 1.7 V, combined with a good stability of more than 100,000 hours at 100 cd/m^2 has been obtained by pure zinc blende CdSe/CdS core/shell HNCs. This design allow obtaining non-blinking single NC emission and, most importantly, excellent reproducible optical properties at ensemble and PL efficiency >90%.

In parallel, graded-shell growth has been demonstrated to improve the structural uniformity in the HNCs and resulting hybrid LED efficiency. The gradual chemical compositional gradient enables effective strain relief, thus improving the material optical properties. Multicolor LEDs with high external quantum efficiencies (14.5% for green, 12.0% for red and 10.7% for blue devices) have been reported by this approach, demonstrating that the fine compositional design could have a preeminent role in determining the final LED performances. Growing a graded ZnSe/ZnS shell in the radial direction has been demonstrate to be a successful strategy to synthesize Cd-free InP/ZnSe while alleviating the lattice strain and protecting the HNCs from degradation.

The quantum confinement regime could be also tuned through shape-design of HNCs. The dot-in-bulk, dot in a rod and double-heterojunction nanorods are examples of shape-design for hybrid LED device purpose. These approaches allow obtaining either white emission or polarized EL, and represent an additional opportunity to improve the PL efficiency.

The effect of shell thickness has been studied to improve solar cell efficiency and photo-stability as well. One of the most limiting factor of NCs based solar cells is represented from charge trapping surface states, which have a deleterious effect manly on Voc values. In PbS/CdS HNCs, the efficient surface passivation of PbS NCs through the CdS shell leads to an increased Voc value compared to the PbS core only. The best device performances are achieved with a CdS shell thickness of 0.1 nm, showing a PCE of 6.05%, a FF of 0.39, Voc 0.65 V and current density of 23.9 mA/cm^2. PbS/CdS HNCs have been also exploited in quantum dot sensitized solar cells as light absorber material. The CdS shell leads to an enhancement of the electron diffusion length and charge collection. Moreover, the shell thickness of quasi type II and type II HNCs can be tailored opportunely to improve carrier separation and extraction for high efficiency solar cell. Solar cells including quasi type II PbSe/PbS HNCs have reached the highest performances obtained with HNCs. The best device exhibits a Jsc of 21.7 mA/cm^2, a Voc of 0.5 V, a FF of 57% and PCE of 6.5%.[9] In addition, type II ZnTe/CdSe have been efficiently used in sensitized solar cell reaching the best PCE of 6.82%.

With the aim of improving the charge separation efficiency, type II CdTe/CdSe HNCs with branched tetrapod shape have been conceived, however the performance of such devices is

limited by the inefficient charge extraction from the HNCs and by the lack of a continuous charge percolation path to the electrodes. Therefore further expedient are required to enhance solar cell efficiency, such as additional layer or ternary hybrid blend.

Albeit the progresses in recent years, there are still rooms to improve the performance of HNC based solar cell device in order to compete with other new generation PV technologies.[127,22] Following the evolution of HNCs for LEDs, PV performance enhancement has to go through the design of HNCs with higher level of complexity, in parallel with the optimization of the solar cell device architecture.

Acknowledgements

The authors gratefully acknowledges SIR Two-Dimensional Colloidal Metal Dichalcogenides based Energy-Conversion Photovoltaics (2D ECO), Bando SIR (Scientific Independence of young Researchers) 2014 MIUR Decreto Direttoriale 23 gennaio 2014 no. 197 (project number RBSI14FYVD, CUP: B82I15000950008) for funding.

Notes and references

1 Z. Hens, *Science*, 2015, **348**, 1211–1212.
2 M. P. Hendricks, M. P. Campos, G. T. Cleveland, I. Jen-La Plante and J. S. Owen, *Science*, 2015, **348**, 1226–1230.
3 D. Liu, X. Xu, Y. Du, X. Qin, Y. Zhang, C. Ma, S. Wen, W. Ren, E. M. Goldys, J. A. Piper, S. Dou, X. Liu and D. Jin, *Nat. Commun.*, 2016, **7**, 1–8.
4 J. I. Saari, M. M. Krause, B. R. Walsh and P. Kambhampati, *Nano Lett.*, 2013, **13**, 722–727.
5 I. C. Lekshmi, R. Buonsanti, C. Nobile, R. Rinaldi, P. D. Cozzoli and G. Maruccio, *ACS Nano*, 2011, **5**, 1731–1738.
6 J. Jang, D. S. Dolzhnikov, W. Liu, S. Nam, M. Shim and D. V. Talapin, *Nano Lett.*, 2015, **15**, 6309–6317.
7 B. Mehdaoui, V. Connord, J. Carrey, P. F. Fazzini, M. Respaud and B. Chaudret, *Nano Lett.*, 2015, **15**, 3241−3248.
8 Y. Yang, Y. Zheng, W. Cao, A. Titov, J. Hyvonen, J. R. Manders, J. Xue, P. H. Holloway and L. Qian, *Nat. Photonics*, 2015, **9**, 259–266.
9 H. Choi, J. H. Song, J. Jang, X. D. Mai, S. Kim and S. Jeong, *Nanoscale*, 2015, **7**, 17473–17481.
10 C. Grivas, C. Li, P. Andreakou, P. Wang, M. Ding, G. Brambilla, L. Manna and P. Lagoudakis, *Nat. Commun.*, 2013, **4**, 2376.
11 I. L. Medintz, H. T. Uyeda, E. R. Goldman and H. Mattoussi, *Nat. Mater.*, 2005, **4**, 435–446.
12 B. Y. X. Lim, *Nature*, 2016, **531**, 26–28.
13 T.-H. Kim, K.-S. Cho, E. K. Lee, S. J. Lee, J. Chae, J. W. Kim, D. H. Kim, J.-Y. Kwon, G. Amaratunga, S. Y. Lee, B. L. Choi, Y. Kuk, J. M. Kim and K. Kim, *Nat. Photonics*, 2011, **5**, 176–182.
14 K. Lee, C. Han, H. Kang, H. Ko, C. Lee, J. Lee, N. Myoung, Y. Sang-Youp and H. Yang, *ACS Nano*, 2015, **9**, 10941–10949.
15 A. Nurmikko, *Nat. Nanotechnol.*, 2015, **10**, 1001–1004.
16 P. V. Kamat, *J. Phys. Chem. Lett.*, 2013, **4**, 3733–3734.
17 L. Carbone and P. D. Cozzoli, *Nano Today*, 2010, **5**, 449–493.
18 V. L. Colvin, M. C. Schlamp and a P. Alivisatos, *Nature*, 1994, **370**, 354–357.
19 X. Dai, Z. Zhang, Y. Jin, Y. Niu, H. Cao, X. Liang, L. Chen, J. Wang and X. Peng, *Nature*, 2014, **515**, 96–99.
20 D. Bozyigit, O. Yarema and V. Wood, *Adv. Funct. Mater.*, 2013, **23**, 3024–3029.
21 D. C. J. Neo, C. Cheng, S. D. Stranks, S. M. Fairclough, J. S. Kim, A. I. Kirkland, J. M. Smith, H. J. Snaith, H. E. Assender and A. A. R. Watt, *Chem. Mater.*, 2014, **26**, 4004–4013.
22 M. V. Kovalenko, *Nat. Nanotechnol.*, 2015, **10**, 994–997.
23 J. Tang, X. Wang, L. Brzozowski, D. A. R. Barkhouse, R. Debnath, L. Levina and E. H. Sargent, *Adv. Mater.*, 2010, **22**, 1398–1402.
24 A. G. Pattantyus-Abraham, I. J. Kramer, A. R. Barkhouse, X. Wang, G. Konstantatos, R. Debnath, L. Levina, I. Raabe, M. K. Nazeeruddin, M. Grätzel and E. H. Sargent, *ACS Nano*, 2010, **4**, 3374–3380.
25 D. A. R. Barkhouse, R. Debnath, I. J. Kramer, D. Zhitomirsky, A. G. Pattantyus-Abraham, L. Levina, L. Etgar, M. Grätzel and E. H. Sargent, *Adv. Mater.*, 2011, **23**, 3134–3138.
26 R. Mastria, A. Rizzo, C. Giansante, D. Ballarini, L. Dominici, O. Inganäs and G. Gigli, *J. Phys. Chem. C*, 2015, **119**, 14972–14979.
27 C. Giansante, R. Mastria, G. Lerario, L. Moretti, I. Kriegel, F. Scotognella, G. Lanzani, S. Carallo, M. Esposito, M. Biasiucci, A. Rizzo and G. Gigli, *Adv. Funct. Mater.*, 2015, **25**, 111–119.
28 S. Giménez, I. Mora-Seró, L. Macor, N. Guijarro, T. Lana-Villarreal, R. Gómez, L. J. Diguna, Q. Shen, T. Toyoda and J. Bisquert, *Nanotechnology*, 2009, **20**, 295204.
29 P. Nagpal and V. I. Klimov, *Nat. Commun.*, 2011, **2**, 486.
30 A. P. Alivisatos, *J. Phys. Chem.*, 1996, **100**, 13226–13239.
31 Mostafa a. El-Sayed, *Acc. Chem. Res*, 2004, **37**, 326–333.
32 P. D. Cozzoli, T. Pellegrino and L. Manna, *Chem. Soc. Rev.*, 2006, **35**, 1195–1208.
33 Y. Yin and A. P. Alivisatos, *Nature*, 2005, **437**, 664–670.
34 A. Fischer, L. Rollny, J. Pan, G. H. Carey, S. M. Thon, S. Hoogland, O. Voznyy, D. Zhitomirsky, J. Y. Kim, O. M. Bakr and E. H. Sargent, *Adv. Mater.*, 2013, **25**, 5742–5749.
35 V. Wood, M. J. Panzer, J. Chen, M. S. Bradley, J. E. Halpert, M. C. Bawendi and V. Bulovic, *Adv. Mater.*, 2009, **21**, 2151–2155.
36 I. J. Kramer, J. C. Minor, G. Moreno-Bautista, L. Rollny, P. Kanjanaboos, D. Kopilovic, S. M. Thon, G. H. Carey, K. W. ei Chou, D. Zhitomirsky, A. Amassian and E. H. Sargent, *Adv. Mater.*, 2015, **27**, 116–121.
37 M. A. Boles, D. Ling, T. Hyeon and D. V Talapin, *Nat. Mater.*, 2016, **15**, 141–153.
38 F. M. Gómez-Campos and M. Califano, *Nano Lett.*, 2012, **12**, 4508–4517.
39 A. a. Bakulin, S. Neutzner, H. J. Bakker, L. Ottaviani, D. Barakel and Z. Chen, *ACS Nano*, 2013, **7**, 8771–8779.
40 J. Aldana, Y. A. Wang and X. Peng, *J. Am. Chem. Soc.*, 2001,

123, 8844–8850.
41 H. M. Zhu and T. Q. Lian, *Energy Environ. Sci.*, 2012, **5**, 9406–9418.
42 S. A. Ivanov, A. Piryatinski, J. Nanda, S. Tretiak, K. R. Zavadil, W. O. Wallace, D. Werder and V. I. Klimov, *J. Am. Chem. Soc.*, 2007, **129**, 11708–11719.
43 C. H. Chuang, S. S. Lo, G. D. Scholes and C. Burda, *J. Phys. Chem. Lett.*, 2010, **1**, 2530–2535.
44 C. de M. Donegá, *Chem. Soc. Rev.*, 2011, **40**, 1512–1546.
45 H. Eshet, M. Grünwald and E. Rabani, *Nano Lett.*, 2013, **13**, 5880–5885.
46 S. J. Lim, B. Chon, T. Joo and S. K. Shin, *J. Phys. Chem. C*, 2008, **112**, 1744–1747.
47 B. O. Dabbousi, J. Rodriguez, F. V Mikulec, J. R. Heine, H. Mattoussi, R. Ober, K. F. Jensen and M. G. Bawendi, *J. Phys. Chem. B*, 1997, **101**, 9463–9475.
48 J. S. Steckel, J. P. Zimmer, S. Coe-Sullivan, N. E. Stott, V. Bulović and M. G. Bawendi, *Angew. Chemie - Int. Ed.*, 2004, **43**, 2154–2158.
49 X. Peng, M. C. Schlamp, A. V Kadavanich and A. P. Alivisatos, *J. Am. Chem. Soc.*, 1997, **7863**, 7019–7029.
50 L. Li and P. Reiss, *J. Am. Chem. Soc.*, 2008, **130**, 11588–11589.
51 M. S. Neo, N. Venkatram, G. S. Li, W. S. Chin and W. Ji, *J. Phys. Chem. C*, 2010, **114**, 18037–18044.
52 L. Qian, Y. Zheng, J. Xue and P. H. Holloway, *Nat. Photonics*, 2011, **5**, 543–548.
53 K.-S. Cho, E. K. Lee, W.-J. Joo, E. Jang, T.-H. Kim, S. J. Lee, S.-J. Kwon, J. Y. Han, B.-K. Kim, B. L. Choi and J. M. Kim, *Nat. Photonics*, 2009, **3**, 341–345.
54 H. Zhu, N. Song, T. Lian and E. U. V, *J. Am. Chem. Soc.*, 2010, 15038–15045.
55 S. Kim, B. Fisher, H.-J. Eisler and M. Bawendi, *J. Am. Chem. Soc.*, 2003, **125**, 11466–11467.
56 D. Dorfs, T. Franzi, R. Osovsky, M. Brumer, E. Lifshitz, T. A. Klar and A. Eychmüller, *Small*, 2008, **4**, 1148–1152.
57 R. Xie, X. Zhong and T. Basche, *Adv. Mater.*, 2005, **17**, 2741–2745.
58 J. He, H. Zhong and G. D. Scholes, *Phys. Rev. Lett.*, 2010, **105**, 1–4.
59 P. T. K. Chin, C. D. M. Donegá, S. S. Van Bavel, S. C. J. Meskers, N. A. J. M. Sommerdijk and R. A. J. Janssen, *J. Am. Chem. Soc.*, 2007, **129**, 14880–14886.
60 S. Kim, Y. T. Lim, E. G. Soltesz, A. M. De Grand, J. Lee, A. Nakayama, J. A. Parker, T. Mihaljevic, R. G. Laurence, D. M. Dor, L. H. Cohn, M. G. Bawendi and J. V Frangioni, *Nat. Biotechnol.*, 2004, **22**, 93–97.
61 I. Swart, Z. Sun, D. Vanmaekelbergh and P. Liljeroth, *Nano Lett.*, 2010, **10**, 1931–1935.
62 D. Yanover, R. Vaxenburg, J. Tilchin, A. Rubin-Brusilovski, G. Zaiats, R. K. Čapek, A. Sashchiuk and E. Lifshitz, *J. Phys. Chem. C*, 2014, **118**, 17001–17009.
63 G. Raino, T. Stoferle, I. Moreels, R. Gomes, J. S. Kamil, Z. Hens and R. F. Mahrt, *ACS Nano*, 2011, **5**, 4031–4036.
64 M. Jones, J. Nedeljkovic, R. J. Ellingson, A. J. Nozik and G. Rumbles, *J. Phys. Chem. B*, 2003, **107**, 11346–11352.
65 M. Jones, S. S. Lo and G. D. Scholes, *Proc. Natl. Acad. Sci. U. S. A.*, 2009, **106**, 3011–3016.
66 V. I. Klimov and D. W. McBranch, *Phys. Rev. B*, 1997, **55**, 13173–13179.
67 M. Califano and F. M. Gómez-Campos, *Nano Lett.*, 2013, **13**, 2047–2052.
68 J. M. Caruge, J. E. Halpert, V. Wood, V. Bulovic and M. G. Bawendi, *Nat Phot.*, 2008, **2**, 247–250.
69 J. E. B. Katari, V. L. Colvin and a. P. Alivisatos, *J. Phys. Chem.*, 1994, **98**, 4109–4117.
70 A. C. Carter, *Phys. Rev. B*, 1997, **55**, 822–828.
71 J. Cui, A. P. Beyler, I. Coropceanu, L. Cleary, T. R. Avila, Y. Chen, J. M. Cordero, S. L. Heathcote, D. K. Harris, O. Chen, J. Cao and M. G. Bawendi, *Nano Lett.*, 2015, **16**, 289–296.
72 F. García-Santamaría, S. Brovelli, R. Viswanatha, J. a Hollingsworth, H. Htoon, S. a Crooker and V. I. Klimov, *Nano Let*, 2011, **11**, 687–693.
73 B. Mahler, P. Spinicelli, S. Buil, X. Quelin, J.-P. Hermier and B. Dubertret, *Nat. Mater.*, 2008, **7**, 659–664.
74 B. N. Pal, Y. Ghosh, S. Brovelli, R. Laocharoensuk, V. I. Klimov, J. a. Hollingsworth and H. Htoon, *Nano Lett.*, 2012, **12**, 331–336.
75 V. Wood, M. J. Panzer, J. E. Halpert, J.-M. Caruge, M. G. Bawendi and V. Bulović, *ACS Nano*, 2009, **3**, 3581–3586.
76 Y. Chen, J. Vela, H. Htoon, J. L. Casson, D. J. Werder, D. a. Bussian, V. I. Klimov and J. a. Hollingsworth, *J. Am. Chem. Soc.*, 2008, **130**, 5026–5027.
77 O. Chen, J. Zhao, V. P. Chauhan, J. Cui, C. Wong, D. K. Harris, H. Wei, H.-S. Han, D. Fukumura, R. K. Jain and M. G. Bawendi, *Nat. Mater.*, 2013, **12**, 445–451.
78 W. Nan, Y. Niu, H. Qin, F. Cui, Y. Yang, R. Lai, W. Lin and X. Peng, *J. Am. Chem. Soc.*, 2012, **134**, 19685–19693.
79 A. Efros, M. Rosen, M. Kuno, M. Nirmal, D. Norris and M. Bawendi, *Phys. Rev. B*, 1996, **54**, 4843–4856.
80 H. Shen, Q. Lin, H. Wang, L. Qian, Y. Yang, A. Titov, J. Hyvonen, Y. Zheng and L. S. Li, *ACS Appl. Mater. Interfaces*, 2013, **5**, 12011–12016.
81 G. J. Supran, K. W. Song, G. W. Hwang, R. E. Correa, J. Scherer, E. A. Dauler, Y. Shirasaki, M. G. Bawendi and V. Bulović, *Adv. Mater.*, 2015, **27**, 1437–1442.
82 B. S. Mashford, M. Stevenson, Z. Popovic, C. Hamilton, Z. Zhou, C. Breen, J. Steckel, V. Bulovic, M. Bawendi, S. Coe-Sullivan and P. T. Kazlas, *Nat. Photonics*, 2013, **7**, 407–412.
83 H. Shen, W. Cao, N. T. Shewmon, C. Yang, L. S. Li and J. Xue, *Nano Lett.*, 2015, **15**, 1211–1216.
84 H. Shen, S. Wang, H. Wang, J. Niu, L. Qian, Y. Yang, A. Titov, J. Hyvonen, Y. Zheng and L. S. Li, *ACS Appl. Mater. Interfaces*, 2013, **5**, 4260–4265.
85 P. O. Anikeeva, J. E. Halpert, M. G. Bawendi and V. Bulović, *Nano Lett.*, 2009, **9**, 2532–2536.
86 J. S. Steckel, P. Snee, S. Coe-Sullivan, J. P. Zimmer, J. E. Halpert, P. Anikeeva, L.-A. Kim, V. Bulovic and M. G. Bawendi, *Angew. Chemie Int. Ed.*, 2006, **45**, 5796–5799.
87 K. H. Lee, J. H. Lee, W. S. Song, H. Ko, C. Lee, J. H. Lee and H. Yang, *ACS Nano*, 2013, **7**, 7295–7302.
88 J. Lim, S. Jun, E. Jang, H. Baik, H. Kim and J. Cho, *Adv. Mater.*, 2007, **19**, 1927–1932.
89 M. V Kovalenko, L. Manna, A. Cabot, Z. Hens, D. V Talapin,

C. R. Kagan, V. I. Klimov, A. L. Rogach, P. Reiss, D. J. Milliron, P. Guyot-Sionnnest, G. Konstantatos, W. J. Parak, T. Hyeon, B. A. Korgel, C. B. Murray and W. Heiss, *ACS Nano*, 1012, **9**, 1012–1057.

90 S. Kim, T. Kim, M. Kang, S. K. Kwak, T. W. Yoo, L. S. Park, I. Yang, S. Hwang, J. E. Lee, S. K. Kim and S. W. Kim, *J. Am. Chem. Soc.*, 2012, **134**, 3804–3809.

91 J. Lim, W. K. Bae, D. Lee, M. K. Nam, J. Jung, C. Lee, K. Char and S. Lee, *Chem. Mater.*, 2011, **23**, 4459–4463.

92 X. Yang, Y. Divayana, D. Zhao, K. Swee Leck, F. Lu, S. Tiam Tan, A. Putu Abiyasa, Y. Zhao, H. Volkan Demir and X. Wei Sun, *Appl. Phys. Lett.*, 2012, **101**, 233110.

93 J. Lim, M. Park, W. K. Bae, D. Lee, S. Lee, C. Lee and K. Char, *ACS Nano*, 2013, **7**, 9019–9026.

94 X. Yang, D. Zhao, K. S. Leck, S. T. Tan, Y. X. Tang, J. Zhao, H. V. Demir and X. W. Sun, *Adv. Mater.*, 2012, **24**, 4180–4185.

95 Z. Zhang, D. Liu, D. Li, K. Huang, Y. Zhang, Z. Shi, R. Xie, M.-Y. Han, Y. Wang and W. Yang, *Chem. Mater.*, 2015, **27**, 1405–1411.

96 Y. Kim, C. Ippen, T. Greco, J. Lee, M. S. Oh, C. J. Han, A. Wedel and J. Kim, *Opt. Mater. Express*, 2014, **4**, 1436.

97 A. Wang, H. Shen, S. Zang, Q. Lin, H. Wang, L. Qian, J. Niu and L. Song Li, *Nanoscale*, 2015, **7**, 2951–2959.

98 Y. Li, A. Rizzo, R. Cingolani and G. Gigli, *Adv. Mater.*, 2006, **18**, 2545–2548.

99 A. Rizzo, M. Mazzeo, M. Biasiucci, R. Cingolani and G. Gigli, *Small*, 2008, **4**, 2143–7.

100 S. Brovelli, W. K. Bae, F. Meinardi, B. Santiago, M. Lorenzon, C. Galland and V. I. Klimov, *Nano Lett.*, 2014, **14**, 3855.

101 S. Brovelli, W. K. Bae, C. Galland, U. Giovanella, F. F. Meinardi and V. I. Klimov, *Nano Lett.*, 2013, **14**, 486–494.

102 M. Zavelani-Rossi, M. G. Lupo, F. Tassone, L. Manna and G. Lanzani, *Nano Lett.*, 2010, **10**, 3142–3150.

103 Z. Zhang, S. Luan, K. Huang, Y. Zhang, Z. Shi, R. Xie and W. Yang, *J. Mater. Chem. C*, 2015, **3**, 3614–3622.

104 L. Carbone, C. Nobile, M. De Giorgi, F. Della Sala, G. Morello, P. Pompa, M. Hytch, E. Snoeck, A. Fiore, I. R. Franchini, M. Nadasan, A. F. Silvestre, L. Chiodo, S. Kudera, R. Cingolani, R. Krahne and L. Manna, *Nano Lett.*, 2007, **7**, 2942–2950.

105 J. L. Baker, A. Widmer-Cooper, M. F. Toney, P. L. Geissler and A. P. Alivisatos, *Nano Lett.*, 2010, **10**, 195–201.

106 L. Li and A. P. Alivisatos, *Phys. Rev. Lett.*, 2003, **90**, 097402.

107 A. Rizzo, C. Nobile, M. Mazzeo, M. De Giorgi, A. Fiore, L. Carbone, R. Cingolani, L. Manna and G. Gigli, *ACS Nano*, 2009, **3**, 1506–1512.

108 A. Castelli, F. Meinardi, M. Pasini, F. Galeotti, V. Pinchetti, M. Lorenzon, L. Manna, I. Moreels, U. Giovanella and S. Brovelli, *Nano Lett.*, 2015, **15**, 5455–5464.

109 N. Oh, S. Nam, Y. Zhai, K. Deshpande, P. Trefonas and M. Shim, *Nat. Commun.*, 2014, **5**, 1–8.

110 S. Nam, N. Oh, Y. Zhai and M. Shim, *ACS Nano*, 2015, **9**, 878–885.

111 B. Mahler, B. Nadal, C. Bouet, G. Patriarche and B. Dubertret, *J. Am. Chem. Soc.*, 2012, **134**, 18591–18598.

112 B. D. Zhuoying Chen, Brice Nadal, Benoit Mahler, Hervé Aubin, *Adv. Funct. Mater.*, 2014, **24**, 295–302.

113 C. A. Leatherdale, W. K. Woo, F. V Mikulec and M. G. Bawendi, *J. Phys. Chem. B*, 2002, **106**, 7619–7622.

114 I. Moreels, K. Lambert, D. Smeets, D. De Muynck, T. Nollet, J. C. Martins, F. Vanhaecke, A. Vantomme, C. Delerue, G. Allan and Z. Hens, *ACS Nano*, 2009, **3**, 3023–3030.

115 W. A. Tisdale, K. J. Williams, B. A. Timp, D. J. Norris, E. S. Aydil and X.-Y. Zhu, *Science (80-.).*, 2010, **328**, 1543–1547.

116 A. J. Nozik, M. C. Beard, J. M. Luther, M. Law, R. J. Ellingson and J. C. Johnson, *Chem. Rev.*, 2010, **110**, 6873–6890.

117 L. Dworak, V. V Matylitsky, V. V Breus, M. Braun and T. Basch, *J. Phys. Chem. C*, 2011, **155**, 3949–3955.

118 H. Zhao, H. Liang, B. A. Gonfa, M. Chaker, T. Ozaki, P. Tijssen, F. Vidal and D. Ma, *Nanoscale*, 2014, **6**, 215–25.

119 H. Zhao, Z. Fan, H. Liang, G. S. Selopal, B. a Gonfa, L. Jin, A. Soudi, D. Cui, F. Enrichi, M. M. Natile, I. Concina, D. Ma, a O. Govorov, F. Rosei and A. Vomiero, *Nanoscale*, 2014, 7004–7011.

120 M. J. Speirs, D. M. Balazs, H.-H. Fang, L.-H. Lai, L. Protesescu, M. V Kovalenko and M. A. Loi, *J. Mater. Chem. A*, 2015, **3**, 1450–1457.

121 L.-H. Lai, L. Protesescu, M. V Kovalenko and M. A. Loi, *Phys. Chem. Chem. Phys.*, 2014, **16**, 736–742.

122 S. Jiao, Q. Shen, I. Mora-Sero, J. Wang, Z. Pan, K. Zhao, Y. Kuga, X. Zhong and and J. Bisquert, *ACS Nano*, 2015, **9**, 908–915.

123 L. Etgar, D. Yanover, R. K. Čapek, R. Vaxenburg, Z. Xue, B. Liu, M. K. Nazeeruddin, E. Lifshitz and M. Grätzel, *Adv. Funct. Mater.*, 2013, **23**, 2736–2741.

124 H. Zhong, Y. Zhou, Y. Yang, C. Yang and Y. Li, *J. Phys. Chem. C*, 2007, **111**, 6538–6543.

125 Y. Li, R. Mastria, A. Fiore, C. Nobile, L. Yin, M. Biasiucci, G. Cheng, A. M. Cucolo, R. Cingolani, L. Manna and G. Gigli, *Adv. Mater.*, 2009, **21**, 4461–4466.

126 S. W. Tong, N. Mishra, C. L. Su, V. Nalla, W. Wu, W. Ji, J. Zhang, Y. Chan and K. P. Loh, *Adv. Funct. Mater.*, 2014, **24**, 1904–1910.

127 A. Mei, X. Li, L. Liu, Z. Ku, T. Liu, Y. Rong, M. Xu, M. Hu, J. Chen, Y. Yang, M. Grätzel and H. Han, *Sci.* , 2014, **345** , 295–298.